SINTA

SImulations of climate chaNge in the mediTerranean Area

FINAL SCIENTIFIC REPORT

S. Gualdi (1,2), B. Rajkovic (3), V. Djurdjevic (3), S. Castellari (1,2),

E. Scoccimarro (1,2) , A. Navarra (1,2) and M. Dacic (4)

(1) *Centro Euro-Mediterraneo per i Cambiamenti Climatici (CMCC)*
(2) *Istituto Nazionale di Geofisica e Vulcanologia (INGV)*
(3) *Belgrade University, Faculty of Physics*
(4) *Republic Hydrometeorological Service of Serbia*

October 2008

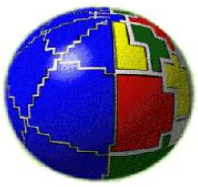

Istituto Nazionale di Geofisica e Vulcanologia

(INGV)

Table of contents

1. INTRODUCTION

1.1 DESCRIPTION OF THE PROJECT AND ITS SCOPE

In the last years several publications in international scientific literature evidenced that the climate change is an ongoing global threat, which causes impacts in different human and natural systems and at global and regional level.

The *Fourth Assessment Report (AR4)* of the *IPCC (Intergovernmental Panel on Climate Change)* in 2007 has shown the large vulnerability of the European region to present and future climate change (**Fig. 1.1**). For the first time, through the analysis of the scientific literature, in Europe wide-ranging impacts of changes in current climate have been clearly analyzed and studied such as longer growing seasons, retreating glaciers, shift of species ranges, and health impacts. These changes have been correlated with those projected for future climate change. The global and regional climate projections shown by the AR4 also provided valuable information on potential future impacts of climate change an most of the European region will be negatively affected. Most probably the climate change will magnify the regional differences in Europe's natural resources and assets.

With a low increase of global mean surface temperature Northern Europe could experience some positive impacts of climate change (reduced demand for heating, increased crop yields and increased forest growth) but as the global warming continues, the impacts could be mostly negative (increased frequency of winter floods, increased number of endangered ecosystems and increasing ground instability).

On the other hand, the Mediterranean area along with Central and Southern Europe (**Table 1.1**) could experience future negative impacts of climate change (high temperatures, drought, acceleration of mountains glaciers retreat), which could cause reduced water availability and consequent hydropower potential, reduced winter tourism on mountains and reduced summer tourism on the coasts, reduced crop productivity, increased health risks due to heat-waves and increased frequency of wildfires.

Among the different European areas, the AR4 (2007) has shown large number of studies especially in North and Central Europe, but a smaller number for the Southern Europe, Mediterranean and the Balkan areas. In particular these areas still lack of regional climate simulations at high horizontal resolution, which could provide adequate information for the estimation of impacts. In fact, the Mediterranean and the Balkan areas are complex geographic areas, which put a clear challenge for the capability of present generation simulation models.

In this SINTA Project two main approaches are used in order to address this important issue of the horizontal resolution in the climate models. The first approach regards the uniform increase of resolution in global models, the other regards the usage of nested models that enhance locally the horizontal resolution. In the former case it is important that

the representation of physical processes are suitable for the level of high resolution that are used, in the latter it is important to a good regional model and appropriate boundary condition.

This SINTA Project addresses both points by establishing a scientific cooperation between the Italian Scientific Institution ***INGV (National Institute of Geophysics and Volcanology)*** and the Serbian Scientific Institutions such as the ***Republic HydroMeteorological Service (RHMSS)*** and the ***University of Belgrade (UB)***. INGV contributes the global models, University of Belgrade and RHMSS contribute their expertise on regional models, parameterization of physical processes and numerical schemes. In particular, the main objectives of this Project are:

1) Perform a set of global simulations with a *Global Climate Model (GCM)* available at INGV;
2) Perform a set of regional simulations with the UB *Regional Climate Model (RCM)* forced by boundary conditions from the GCM simulations;
3) Test the convection parameterization developed at UB in the INGV global model;
4) Training and visit exchanges of Serbian scientists in Italy.

The **Scientifc Coordinator** of SINTA Project and **Contact Point** is Sergio Castellari (INGV,CMCC).

1.2 DESCRIPTION OF THE PROBLEM

Since the early nineties, starting with work of Giorgi (1989) and later followed by series of papers (1900, 1991 a,b, 1993 a,b, 1994, 1996 a,b,2004 I,II) and by other numerous authors (Jones et al, 1997, Ekman AML and Rodhe H ,2003, Räisänen et al, 2004 among others), high resolution limited domain models have been nested into low resolutions global models. Such models become known as *Regional Climate Models (CRCM)*. The idea was that regional models with much higher resolution will improve global results by improving at least forcing at the surface-atmosphere interface. Beside that, a regional model may have improved parameterizations of various physical processes in comparison with the respective parameterizations of the global model. The biggest differences are in representations of the topography, land-sea contrast and surface characteristics of the land, such as soil types and soil vegetation.

In **Fig. 1.2** are shown of differences in topography representation for four different horizontal resolutions. Top left for the 400 km grid, resolution of the global models in the 1960s, top right 100 km grid, resolution of the present global models, bottom right 25 km grid, resolution of CRCM and bottom left 10 km grid (the next generation of global models in the optimistic view on the model development). Since we know that large part of the climate forcing comes from the land-sea-air interactions we expect that this, higher horizontal resolution, will improve CRCM simulations in comparison with the global ones. Of course there are obvious limits in these improvements. If GCM has a large bias in

representing the large scale fields, on horizontal scales larger than the domain of the CRCM, then that cannot be corrected by the CRCM. On the other hand where forcing is local we do hope to improve possible biases of the GCM simulations. In our case improvement could be expected t from the new sea/ocean SST since SINTEXG has low resolution in the Mediterranean Sea, the main sea that influences the Italy and Balkan region.

2. MODELS AND DATA

In this Section a brief description of the main characteristics of the models, both global and regional, and of the observational data used in the study is given.

2.1 THE GLOBAL MODEL

The global modelling data employed in this work are time series obtained from climate simulations carried out with the SINTEX-G (SXG) coupled atmosphere-ocean general circulation model (AOGCM), which is an evolution of the SINTEX and SINTEX-F models (Gualdi et al., 2003a, 2003b; Guilyardi et al., 2003, Luo et al. 2004, Masson et al. 2005, Behera et al. 2005). The ocean model component is the reference version 8.2 of the Ocean Parallelise (OPA; Madec et al. 1998) with the ORCA2 configuration. To avoid the singularity at the North Pole, it has been transferred to two poles located in Asia and North America. The model longitude- latitude resolution is 2°x 2° cosine (latitude) with increased meridional resolutions to 0.5° near the equator. The model has 31 vertical levels, ten of which lie in the upper 100 metres of the ocean. Model physics includes a free-surface configuration (Roullet and Madec 2000) and the Gent and McWilliams (1990) scheme for isopycnal mixing. Horizontal eddy viscosity coefficient in open oceans varies from 40000 m^2s^{-1} in high latitudes to 2000 m^2s^{-1} in the equator. Vertical eddy diffusivity and viscosity coefficients are calculated from a 1.5-order turbulent closure scheme (Blanke and Delecluse 1993). For more details about the ocean model and its performance, readers are referred to Madec et al. (1998) or online to the web-site http://www.lodyc.jussieu.fr/opa/.

The evolution of the sea ice is described by the LIM (Louvain-La-Neuve sea ice model; Fichefet and Morales Maqueda, 1999), which is a thermodynamic-dynamic snow-sea ice model, with three vertical levels (one for snow and two for ice). The model allows for the presence of leads within the ice pack. Vertical and lateral growth and decay rates of the ice are obtained from prognostic energy budgets at both the bottom and surface boundaries of the snow-ice cover and in leads. When the snow load is sufficiently large to depress the snow-ice interface under the sea-water level, seawater is supposed to infiltrate the entirety of the submerged snow and to freeze there, forming a snow ice cap. For the momentum balance, sea ice is considered as a two-dimensional continuum in dynamical interaction with the atmosphere and ocean. The ice momentum equation is solved on the same horizontal grid as the ocean model. LIM has been thoroughly validated for both Arctic and

Antarctic conditions, and has been used in a number of process studies and coupled simulations (Timmermann et al. 2005 and references therein).

The atmospheric model component is the latest version of ECHAM-4 (Roeckner et al. 1996). We adopted a horizontal resolution T106, corresponding to a gaussian grid of about 1.12° x 1.12°. In the pantheon of long coupled climate simulations, this is a considerably high horizontal resolution. A hybrid sigma-pressure vertical coordinate is used with 19 vertical levels. The parameterization of convection is based on the mass flux concept (Tiedtke, 1989), modified following Nordeng (1994). The Morcrette (1991) radiation scheme is used with the insertion of greenhouse gases (GHGs) and a revised parameterization for the water vapor and the optical properties of clouds. A detailed discussion of the model physics and performances can be found in Roeckner et al. (1996).

The ocean and atmosphere components exchange SST, surface momentum, heat and water fluxes every 1.5 hours. The coupling and the interpolation of the coupling fields is made through the OASIS2.4 coupler (Valcke et al., 2000). No flux corrections are applied to the coupled model.

2.2 THE REGIONAL MODEL

The regional climate model that was used in this project is a combination of two limited area models one for the atmosphere and the other one for the ocean. The reason for the inclusion of the ocean model into CRCM is that the scope of the project was the region of the southern Europe, Italy and Balkan Peninsula. Both are surrounded by the Mediterranean Sea and presumably influenced by it.

The atmospheric component was the limited area model developed by Janjić. The model has two versions of the vertical coordinate system. The original σ, orography following system and η, quasi-horizontal coordinate system introduced by Mesinger (1984, 1988). In our simulations we kept the η choice of the vertical coordinate (Eta in the further text). This model was originally developed in Belgrade and latter improved and operationally used at NCEP. For details of the model please see papers by Janjić (1977, 1979, 1989, 1990, 1994, 1999) and Mesinger (1988).

To insure good representation of the geostrophic adjustment process, model is on the E-grid, Winninghoff (1968), Arakawa and Lamb (1977) nomenclature. Its dynamic core has conservative advection scheme for all variables and efficient time stepping through splitting of the fast processes (geostrophic adjustment etc.) and slower ones advection and physics in general.

The physics package consists of surface scheme, radiation scheme (Fels and Schwarzkopf, 1975), turbulence closure sub model, viscous sub-layer and convection parameterization. The centre of atmospheric model was at 16E, 42.5N and the horizontal resolution was 0.25 degrees. In vertical direction model had 32 levels, with first level at 20 meters, while the top was at 10 mb. The standard radiation scheme assumes that the

composition of the atmosphere is constant with several possibilities of the amount of CO_2. In our runs profiles of the greenhouse gasses was as in the A1B scenario, which means changing of the CO_2 amount from the present value to roughly $2xCO_2$. So we took another radiation scheme that was kindly provided to us by Dr. Carlos Pérez from the Barcelona Supercomputing Center, Earth Sciences Division, Barcelona, Spain, (Carlos et al, 2006) which had the option of variable content of the greenhouse gasses. We have improved its part that does connection between radiation and clouds. After some adjustment we were relatively satisfied with its performance.

The ocean component is the Princeton ocean model (POM), a three-dimensional, primitive equation, numerical model, developed by Blumberg and Mellor and (1987). A comprehensive description of POM can be found in Mellor (2002). Its principal attributes are: horizontal grid uses curvilinear orthogonal coordinates on the C-grid (Arakawa and Winninghoff nomenclature), vertical coordinate is σ coordinate, efficient time differencing (explicit in horizontal and implicit in vertical), free surface, complete thermodynamic and has imbedded second order turbulence closure (Mellor-Yamada 2.5, 1983). Advection schemes use the finite volume approach which is particularly suitable for the case of the curvilinear orthogonal coordinates.

Important part of every coupled model is method of exchange of data between its two components. Due to very different geometries of the two components of the model special care was taken in design of this coupling module.

In **Fig. 2.1** we present schematic representation of overlapping of the two grids in the model. Beside different positions of the corresponding points there is difference in horizontal resolution. Roughly, the atmospheric component had four times coarser resolution. That led to different land-sea masks two components with slightly different distributions of sea and land. A same point can be seen as a land point and for the atmospheric component and ocean point by the ocean model. Then, due to large differences in heat and momentum fluxes over land and sea, energy and momentum exchange between sea and atmosphere will be wrong. To avoid such situation ocean points are separated in two categories. The first category consists of the points that are seen as ocean points in both atmosphere and ocean component. The ocean points, that are seen as land points by the atmosphere component, are the second category. Fluxes at such points were computed in the following way. First we assign the value of the average flux, averaging done over all points in the first category. In order to avoid possible jumps, at the edge of the two sets of points, laplacian smoothing is applied over the second set of points. Relative positions of the both models are shown in **Fig. 2.2** with atmospheric model domain (Eta) light blue and the POM domain dark blue. This system we will call CRCM in the further text. Models exchange fluxes and SST every physical time step of the atmospheric model, which was in these runs 180 seconds.

Our main regions of interest are the Apennine and Balkan Peninsula which are surrounded by the various seas, parts on the Mediterranean Sea and Black Sea. While the whole Mediterranean Sea was inside of POM's domain, Black Sea and parts of the Atlantic

were not. The SST of those water bodies were the one from the GCM. Our Mediterranean Sea was closed on both Gibraltar and Dardanelles

Even though SINTEXG's ocean component has increased horizontal resolution over Mediterranean of 1x1 deg latitude longitude which is twice the resolution of the rest of the world ocean it still should be higher.

The first step in nesting a CRCM into a global model's domain is development of an interface between them. Such interface brings fields from the GCM to CRCM domain using some interpolation technique. There s is also a technical question of formats between the two models. The SINTEXQ model has outputs in the NetCDF format with files that covers one month of integration. So first, set of shells and programs was developed that read the NetCDF formatted files and did some checking of the correctness of the procedure. Once files being decoded, all relevant fields were interpolated to Eta's grid. After the space interpolation, linear interpolation time was done in which fields with 6 hours time interval where interpolated to 6 minutes interval which is the length of the atmospheric time step.

For the verification of the present climate we used two data sets:

1) the *CRU CL 1.0 data set* (Climatic Research Unit - School of Environmental Sciences University of East Anglia Norwich), which is 0.5x0.5 degrees global climatology fields covering 1960-1991 (New et al, 1999, 2000 and 2002);

2) the *Willmott and Matsura data set* (Willmott, Matsuura and Collaborators' Global Climate Resource, Center for Climatic Research Department of Geography University of Delaware). (Willmott and Matsuura, 2001)

The Global Air Temperature and Precipitation were re-interpolated and documented by Cort J. Willmott, Kenji Matsuura and David R. Legate: That data set has re-girded monthly and Annual Climatologies. Legates and Willmott's (1990a and b) station records of monthly and annual mean air temperature (T) and precipitation (P) were used to produce this archive. The number of stations (and oceanic grid nodes) used was 24,941 for air temperature, and 26,858 for precipitation, respectively. Data has .5x.5 degrees global coverage.

Beside these two surface fields we have examined geopotential height at 500 mb and in the case of present climate, compared it with the NCEP's reanalysis (The NCEP/NCAR Reanalysis Project at the NOAA/ESRL). It'sTemporal Coverage is 4-times daily, with monthly values for 1948/01/01 to present. Spatial coverage is global, with 17 pressure levels and 28 sigma levels. It covers period from 1948 to the present.

2.3 THE REFERENCE DATA

The simulated climate of the Euro-Mediterranean region and the main features of its variability are evaluated comparing the model results with observational data sets.

Specifically, we use data from the ECMWF 40-year Re-Analysis (ERA40; more information available at the web- site *http://www.ecmwf.int/research/era*), and the observed precipitation from the Climate Research Unit (CRU) data set (Jones et al. 2006). For the sake of simplicity, in the rest of the paper we will refer to all of these data as observations.

3. THE GLOBAL SIMULATIONS

With respect to the previous versions of the SINTEX model, SXG includes a model of the sea ice, which allows the production of fully coupled climate scenario experiments. In this paper, we present results obtained from the analysis of two climate simulations. In order to assess the capability of the model to reproduce a reasonably realistic Euro-Mediterranean climate, 30 years (1961-1990) of a twentieth century simulation (20C3M) have been analyzed and compared with observations. The simulation (hereafter referred to as 20C) has been conducted integrating the model with forcing agents, which include greenhouse gases (CO2 , CH4 , N2O and CFCs) and sulfate aerosols, as specified in the protocol for the 20C3M experiment defined for the IPCC simulations (for more details see also the web-site *http://www-pcmdi.llnl.gov/ipcc/about ipcc.php*). The integration starts from an equilibrium state obtained from a long coupled simulation of the pre-industrial climate, and has been conducted for the whole period 1870-2000.

Once the skill of the model to reproduce Euro-Mediterranean climate has been evaluated using the present climate simulation, the possible changes induced by greenhouse global warming have been explored using the last 30 years of data from a 21st Century climate scenario experiment. Specifically, the climate scenario simulation here considered has been performed integrating the model with forcing agents, greenhouse gases (GHGs) and sulphate aerosols, evolving as specified in the protocol for the A1B SRES experiment defined for the IPCC simulations (*http://www-pcmdi.llnl.gov/ipcc/about ipcc.php*). In the A1B simulation, the model starts from the last simulated day of the C20 integration and is integrated for 100 years. The data analysed in this study are obtained from the last 30 years (2071-2100) of the scenario simulation.

Fig. 3.1 shows the time series of the annual mean values of surface temperature averaged over all latitudes and longitudes, from year 1870 to year 2100, for the model simulation (solid curve). Along with the simulated surface temperature, the observed global average surface temperature (Jones et al. 2001) is also shown for the period 1870-2000 (dashed curve). The curves represent the year-to-year deviation of the annual mean with respect to the 1870-1890 mean. The observations (dashed curve) show the well known global warming trend of about 0.6°C over the past century. The model simulation (solid curve) exhibits a similar trend, albeit slightly more pronounced, over the same period. Analogous results are found for the sea-surface temperature (SST) field (not shown). During the period 2001-2100, the simulated surface temperature exhibits a more substantial increase. During the last 30 years of the 21st century, the mean surface temperature deviation with respect to the 1961-1990 mean exceeds 2.5°C. This result is

fully consistent with the results obtained from A1B scenario climate simulations performed with other models (IPCC-AR4 2007).

Fig. 3.1 gives an estimate of the warming of the surface temperature, due to the increase of the GHGs and aerosol concentration, on global scale. However, in order to better understand the mechanisms that drive the climate change and to plan policies of adaptation and mitigation of its effects, it is very important to have a detailed description of the change of the main physical parameters on regional scale. This analysis will be performed in the next Section.

3.1 ANALYSIS OF THE 20C SIMULATION, COMPARISON WITH THE OBSERVATIONS

Before to discuss the characteristics of the climate change due to the increase of GHGs concentration in the Earth atmosphere as simulated by the model, we analyse the skill of the model to reproduce a realistic climate. To this aim, we compare the seasonal means and the basic features of the variability of (sea-)surface temperature, precipitation and low level wind velocity as obtained from the observations and the 20C simulation for the period 1961-1990.

3.1.1 MEAN SEASONAL CYCLE

Fig. 3.2 shows the seasonal means of seas-surface temperature (SST) and precipitation as obtained from the observations and the 20C model simulation, for the extended northern summer (June-October, JJASO) and southern (December-April, DJFMA) summers. The seasonal means have been calculated for the period 1961-1990 both for the observed and model data.

Overall, the model appears to be reasonably good in reproducing the observed seasonal mean fields. In the Tropics, the model tends to overestimate the SST for both seasons. The seasonal mean SST averaged over the Tropics (23.5°S-23.5°N) is 0.26°C and 0.32°C warmer than observed in JJASO and in DJFMA respectively. The warm bias is visible in both the tropical Indian Ocean and in the Atlantic Ocean and it is particularly evident in the central-eastern Pacific, south of the equator. In this region, over the warm SSTs the model also overestimates the rainfall, tending to produce a double ITCZ, which is a common error of most AOGCMs. In the equatorial Pacific, on the other hand, the model cold tongue is clearly too strong and extends too far west. Correspondingly, the simulated precipitation is too weak in the equatorial Pacific, especially west of the date line.

In the tropical Atlantic, the model rainfall is reasonably close to observations in JJASO, whereas during DJFMA it appears to be shifted south (by about 10° of latitude), probably as a consequence of the excessively warm SSTs found in the subtropical southern Atlantic, off the Brazilian coast. Interestingly, in the tropical Indian Ocean, the model precipitation is

generally weaker than observed. During the northern summer, the model shows a clear rainfall deficit in the area affected by the Asian summer monsoon, extending from the Bay of Bengal, through South-East Asia and the South China Sea, up to the region east of the Philippines archipelago. Simulated precipitation also appears to be too weak over the eastern equatorial Indian Ocean, whereas it tends to be too intense in the western part of the basin, between the equator and 10°S. During the northern winter (**Fig. 3.2**, panels g and h) model rainfall is too weak over the eastern Indian Ocean and the Indonesian region.

In the extratropical Northern Hemisphere, during both boreal winter and summer, the model SST is too warm in the North Pacific and North Atlantic, in the storm track region, and in the Labrador Sea. In the Southern Hemisphere, too warm SST is simulated in the storm track region. The simulated precipitation exhibits some substantial bias in the mid-latitude of the Southern Hemisphere during austral winter. During the same season, the simulated precipitation appears to be deficient over Europe, Japan and the western side of the Asian continent.

Since in this study we are particularly interested in the Euro-Mediterranean region, we focus now on the climatic features of this area. **Fig. 3.3** shows the seasonal means of the 2-metres temperature (T2m) obtained from the observations (left panels) and the 20C simulation (right panels). In order to emphasize the regional characteristics of the seasonal cycle, the mean northern autumn (October-December, OND), northern winter (January-March, JFM), northern spring (April-June, AMJ) and northern summer (July-September, JAS) are shown.

Overall the main features of the T_{2m} seasonal cycle appear to be well reproduced by the model. However, some remarkable difference between the observed and the simulated seasonal cycle is clearly visible. For example, the observed surface air temperature appears to be generally colder than in the simulation, especially in the central and northern eastern Europe. The model, on the other hand, appears to be slightly cooler in the mountain regions, such as, for example, the Alps, the eastern Anatolia and the Caucasian Range, the Atlas mountains, particularly in boreal autumn and winter (**Fig. 3.3**, panels e and f).

Also the simulated seasonal means of precipitation show some bias compared to observations (**Fig. 3.4**, shaded patterns). The main difference concerns the phase of the seasonal cycle of the precipitation in the central and northern-eastern Europe. In the observations, the largest precipitation in these regions is found during northern summer and autumn (**Fig. 3.4**, panels d and a), whereas during northern winter and spring rainfall has a minimum. In the model simulation, on the other hand, the most intense precipitation in these areas is found during boreal autumn and spring (**Fig. 3.4**, panels e and f), whereas in spring and summer it has a minimum (Figure 4, panels d and h)

Fig. 3.4 shows also the seasonal cycle of the 850 hPa wind velocity (arrows). Also in this case, the model appears to reproduce well the main, gross features of the low-level flow, though some difference with the observations is visible. In particular, the simulated

wind appears to be generally lightly stronger than observed over the European continent, especially its zonal component.

An important feature of the mid-latitude climate of the Northern Hemisphere are the stationary waves, which appear evident in the eddy component of the 500 hPa geopotential height (Z500). **Fig. 3.5** shows the seasonal means of the eddy Z500 for the observations (left column) and the model (right column). The main features of the observed stationary waves and of their seasonal modulation are well captured by the model. The amplitude of the simulated is fairly realistic, even if slightly overestimated over the Atlantic sector.

3.1.2 MEAN VARIABILITY

So far, we have assessed the model ability to simulate the 20th Century climate in terms of seasonal means. However, in order to give a more complete evaluation of the model performance, now we compare the observed and simulated climate variability. A first gross assessment of the simulated variability can be given by comparing the patterns of standard deviation (STD) of the main physical parameters as obtained from the model and from the observations.

Fig. 3.6 exhibits the STD of the seasonal values of T_{2m} for the observations and the model. Both in the model and observations, the largest variability is found during boreal autumn and winter in the north-eastern part of the considered domain. Even if the model has a slight tendency to overestimate the variability of the T_{2m}, the patterns and the seasonal modulation of the variance appear to be well reproduced.

The variability of the precipitation field is shown in **Fig. 3.7**. In this case, the model captures the locations where the maxima of variability of the observed precipitation are found, such as the Alps region, the western part of the Iberian Peninsula and Scandinavia. Relative maxima of variability of the simulated rainfall are also found over the western part of the Balkans, Turkey and over the Caucasian region, though they appear to be much weaker than in the observations. Noteworthy, the model does not simulate the large variability of precipitation observed over the north-western part of the British Island throughout the year

Fig. 3.8 shows the seasonal modulation of the variability of the eddy component of Z500 in the Northern Hemisphere. Consistent with the observations, the model produces the largest variability over North Pacific, North Atlantic and the northern part of Siberia during boreal autumn and winter. During boreal spring and summer the variability of the Z500 appears to be much weaker, both in the model and observations, suggesting a marked reduction of the variability of the stationary waves.

The results shown in **Figs. 3.2-3.8** indicate that the model is able to simulate a reasonably realistic climate of the Euro-Mediterranean region for the period 1961-1990. In general, the simulated mean seasonal cycle of the principal physical parameters that

characterize the surface climate is in good agreement with the observations. Furthermore, also the main basic features of the mean seasonal variability produced by the model are consistent with the results found from the observations. Therefore, it is of interest to analyse what are the main changes that the model produces when a scenario simulation of the 21st Century is compared with a simulation of the 20th Century. In the next Section, the mean features of the seasonal means obtained from the simulated 1961-1990 climate will be compared with seasonal means for the period 2071-2100 obtained from the A1B scenario simulation.

3.2 COMPARISON BETWEEN THE 20C AND A1B SCENARIO SIMULATIONS

Fig. 3.9 shows the differences between the seasonal means of T_{2m} (left column) and precipitation (right column) as obtained from the 20C and the A1B scenario simulation. The mean have been computed for the period 1961-1990 and 2071-2100 respectively and the picture shows the difference A1B-20C. Overall, the A1B T2m is substantially warmer over the entire Euro-Mediterranean region. The warming is largest in the northern part of the domain and especially over the north-east Europe from autumn to spring, whereas during boreal summer, the largest warming is located over southern Europe and the Mediterranean region, where it appears to exceed 5°C.

In contrast with T_{2m}, precipitation does not exhibit a uniform change between the 20C and the A1B simulation. During the northern autumn and winter, in fact, the rainfall appears to increase over northern Europe and decrease over the southern part of the continent and the Mediterranean region. In boreal spring and summer, on the other hand, most of the Euro-Mediterranean is characterized by a decrease of precipitation in the A1B experiment, with a slight increase mostly confined at very high latitudes (northern than 60°N).

Therefore, according with the A1B scenario, the southern part of Europe and the Mediterranean region during the late part of the 21st Century could be characterized by a substantially hotter climate during summer and drier conditions, particularly intense during the autumn and winter seasons. In some part of the Iberian Peninsula, Alpine region, Italy and on the western Balkans, the reduction of rainfall might be considerably strong, larger than 1 mm/day, which represents a depletion of about 20% of the mean precipitation found during the 1961-1990 period. These findings are fully consistent with the results obtained with numerous other models (e.g., IPCC-AR4 2007) and thus they appear to be very robust.

The climate change revealed by the results shown in **Fig. 3.9** is not limited to the seasonal means. Figure 10 shows the standard deviation of the seasonal values of T_{2m} and rainfall obtained from the A1B integration. These results, compared with **Fig. 3.6** and **Fig. 3.7** indicate that in general the variability of the near-surface air temperature tends to decrease during autumn and winter and to increase during spring and summer.

Interestingly, the summer increase of T_{2m} variability appears to be more pronounced over south-western and central Europe and the Balkans. Also the variability of precipitation (**Fig. 3.11**, right panels) and of the eddy Z500 (**Fig. 3.12**, right panels) appear to be decreased in the A1B climate. The reduced variability of rainfall is visible especially in the Iberian Peninsula and southern France, whereas the variability of the stationary waves appears to be weaker over the North Atlantic in autumn and winter.

Many of the results shown so far indicate that southern Europe and the Mediterranean region exhibit a sometime markedly different behaviour compared with northern Europe. The different characters of these two parts of our domain (the Euro-Mediterranean) appear particularly evident when the differences between the 20C and the A1B integrations are analysed, both in terms of seasonal means and variability. Therefore, it is of interest to explore more in detail what are the possible differences between the two climate simulations in the two regions separately. To this aim, we define the north-central Europe (NCE) region as the area included between 50°N-60°N and 10°W-50°W, and the southern Europe-Mediterranean (SEM) region as the area included between 30°N-45°N and 10°W-50°E.

In order to estimate the possible changes in the distribution of the seasonal values of T_{2m} in the A1B climate scenario in the CEN and SEM regions, **Fig. 3.12** shows the distribution of the seasonal means of the near-surface air temperature as obtained from the 20C experiment (red bars) and the A1B scenario simulation (green bars). In general, the agreement between the distributions obtained from the observations (not shown) and the 20C simulation is reasonably good, though in summer the model appears to be warmer than the observations in both regions, consistent with **Fig. 3.3**.

4. REGIONAL SIMULATIONS

4.1 DESCRIPTION OF THE EXPERIMENTAL SET-UP

We have performed two time slice integrations, the present climate (1960-1990) and the end of the 21st century (2070-2100). The initial fields for the atmosphere were obtained from the global runs as well as the boundary conditions. Updating at the boundaries was done every 6 hours according to the boundary conditions of the Eta model. If the flow was entering the domain, at the first row of points values are read in. In the second row of points we had diagonal averaging between the points of the first row and the points of the third row where model did calculate. If the boundary point is an out flow point model had the upstream advection from its inside over boundary 4-5 points.

The ocean points were initialized with the MODB (Mediterranean Ocean Data Base) data set (Brasseur et al, 1996) the monthly climatology of the Mediterranean Sea. Over Atlantic and Black Sea SST was initialized interpolating it from the SST of the global model.

In the case of the future climate both atmosphere and ocean were initialized from the global model.

4.2 ANALYSIS OF THE 20TH CENTURY SIMULATION

The first step in establishing the quality of a climate model is comparison of it's simulations with the observed climatologies. To do that we present seasonal means for the winter and summer seasons (DJF and SSA in the further text) from our CRCM and corresponding fields from the CRU data set. The first group present two meter temperature (T_{2m} in the further text) for the DFJ season, with top left panel showing temperature from the CRCM, top left the same from the CRU data set, bottom left global filed and bottom right panel has scores in the form of *bias* (Averaged difference), *mae* (Mean absolute) and *rmse* (Rot mean square error difference between the CRCM and CRU data).

First we can say that there is a general agreement between CRCM and CRU except in the North-east part where CRCM has larger T2m. Going from region to region we see that North Africa is captured very well and similar for Spain. The Pyrenees are visible in both data sets, even "better" in the CRCM meaning more refined fields coming from the higher resolution of the CRCM. For France similar situation with prominent region of Alps in both data sets. Italy, north and central are well captured with Sicily slightly cooler by 1 degree. The western Balkan and Albania shows quite good resemblance between the two data sets. Going to the North-east situation gets worse, as mentioned at the beginning. To the South, Greece and Turkey, we are back to the previous level of accuracy. The global fields do capture general structure with closer resemblance in the west part of the domain but being warmer to the North-east. Alps are still the region with the strongest signal. Due to the smaller scale mountains like Primes and Carpathians are less prominent. Italy is warmer at least 1-3 degrees increasing going to the South. Over Balkans agreement is relatively good having in mind the differences in the horizontal resolutions. Turkey similarly is captured well while Greece is slightly warmer, more to the South. In numbers *bias* score is -0.21, *mae* is 1.88 and *rmese* is 2.15, numbers quite similar to the one reported in literature. In the next figure, **Fig.4.2**, we show results for the summer season in the same order of panels.

Both global and CRCM simulations are warmer than the verification but general resemblance is present. Again west is better then the east. Actually the shape of the of T2m fields from CRCM and CRU scale quite good. This is also visible from the scores, which are worse than fore the winter season but still quite acceptable for the climate simulations. Closely connected with temperature fields are the geopotential fields which we verified against the ERA-40 data set.

Comparison between CRCM and reanalysis fields show similarity in shape except that CRCM lines are shifted to the north reflecting the warmer atmosphere in the CRCM simulations. That tendency is also visible in the global runs to a larger degree. So here we have the case of a bias in the global simulations that is reduced in the CRCM simulations.

Also the shapes of the iso-lines in the global runs show unphysical waviness that is not present neither in the reanalysis nor in the CRCM results.

The summer results, presented in **Fig. 4.3** show clearly the excessive warming in the eastern part of the domain since the reduction of the gradient in geopotential reflects warmer 1000-500 mb layer.

Next we turn to the precipitation verifications. **Figs. 4.5** and **4.6** and have winter and summer seasonal averages of the precipitations respectively. Positions of the extreme precipitation over Alps and on the Eastern Adriatic coast is captured but the values are larger in the CRCM simulations then the observed. In general one should not “argue” with the observations but in this case, of the precipitation, maybe the CRCM results are closer to the reality then the CRU data set. In particular the Montenegro coast maximum looks reasonable since we know that we have the Europe maximum in precipitation in the winter season.

On the other hand the south Turkish coast maximum is missing in the CRCM results. Also the North Africa, coast of Allegers has to narrow precipitation zone which is missing in the eastern Libya coastal region. The global simulations are quite smooth with indications of Alps and Adriatic coast maxims. For the summer season we get reduction of the precipitation thought the integration region which is consistent with the higher T2m temperatures earlier documented.

Maximum over Alps is present but is narrower and weaker then in the observations. To the east of Alps there is even larger decrease particularly over Hungary and over Carpathians as well. Unfortunately the CRU data set has only land measurements so we cannot verify precipitation over sea. Still we can notice that there are differences in the precipitation over sea between the CRCM and GCM runs. The CRCM run shows smaller precipitation all over Mediterranean Sea, Turkey and Black Sea, while in the GCM runs that zone is moved much further to the South over Northern Africa.

The last parameter that we will analyze is the 10 meter wind. Unlike in the case of precipitation and surface temperature it is not clear how to present climatology of the wind, especially its orientation. We choose to present wind filed using the stream function and coloring from weak winds in purple to strongest wind in red. Now we just compare CRCM and GCM simulations again for the winter and the summer season. They are presented in the **Figs. 4.7** and **4.8**. Starting with DJF season we see that in the CRCM simulation we see clearly positioning of the local winds according to the orography/land-sea distribution.

For instance the Rhone valley or Ionian/Aegean winds. Global runs are less variable, practically homogenous fields over the sea with intensification over North-western Europe but still weaker then in the CRCM runs. On the other hand over the Mediterranean Sea global runs have uniform fields, stronger then the winds from CRCM in the area of the Western Mediterranean. Similar situation is over the Black Sea. Global fields are more homogenous and stronger in comparison with the corresponding CRCM winds.

Coming to the summer season same general conclusion stands. Global runs have less variability, again stronger winds in the Western Mediterranean area and the Black Sea area. On the other hand CRCM runs have the Ionian/Aegean winds stronger then the global runs. The Rhone valley signal is weaker but the winds in the Alboran Sea are still visible.

4.3 COMPARISON BETWEEN 20TH CENTURY (1960-1990) AND A1B SCENARIO OF THE 21ST CENTURY (2070-2100)

The results from climate simulations are presented as differences of 30 year means between future climate (2007-2100) and present climate (1961-1990). The 30 year means should be able to capture 75% of the variance of the true signal according to, Huntingford et al. (2003) as well as statistically significant changes in extreme precipitation. We present these differences for DJF and JJA seasons for three main parameters, T2m, precipitation, and surface wind.

4.3.1 THE SURFACE TEMPERATURE FIELD

We start with T2m fields. In **Fig. 4.8**, top panels, present differences from the CRCM simulations, with the DJF season on the left and JJA season on the right and global simulations in bottom panels, for the same two seasons. For the CRCM simulations the range of changes is between 1.2-3.5 degrees for the DJF season while for the JJA season are larger and are in the range of 1.8-4.2 degrees. Larger values are connected either to the local topography, Alps, Pyrenees, Balkan Mountains, and Apennines or like for the Italy with both topography as land-sea line. The same holds in the case of the southern edge of the Turkish Plato. Two maximums with strongest warming, for the DJF, occur over the Alps region, with almost 3.5 degrees, and north-eastern region of the southern Alger n corner of the domain. The weakest warming is over Aegean Sea and in Africa in Sahara around 30 degrees North and 5 degrees East.

Looking at the SST over the Mediterranean Sea, the Aegean Sea shows the smallest while north-western Mediterranean has the largest SST increase. In the rest of the domain variations are from about 1.5 to 2.2 degrees. Several warmer spots are in Spain, over Prokletije Mountains in the northern Albania and in the western Morocco.

In the SINTEXG simulations area near Alps has weak gradients, while it is quite strong in the north-eastern corner of the domain. As we said before that is probably error in the global model runs but which has been partially *reduced* in the regional simulations.

Coming to the next, JJA season, we see now clear difference over whole African domain. Where in the previous season we had very weak signal now it is quite clear with magnitude of 2.5-3 degrees. Southern Spain is warmer by about 2.5 and the rest of the central Spain about 2.4. Only near Pyrenees, to the south of them, we have warming of

about 2 degrees. The Pyrenees itself shows again strong signal. The same holds for the Alps which are again the warmest region. Central and southern Italy has much larger increase than during the DJF season with the exception of the Po river valley. The whole of Balkans are warmer from 2.2-2.6 degrees with even larger warming over mountains. Edge of the Turkish Plato next to the Mediterranean shows the strongest signal with magnitude over 3 degrees. The rest of Turkey show also quite large increase of about 2.7 degrees. During the JJA season Sahara has the maximum increase of 4.2 which extends thru ought Allegers. Alps, Pyrenees, Central France and almost over the whole Italy together with western Balkans are the warmest area in Europe.

Most of the Mediterranean Sea is warmer by about 2 degrees. Area between Algiers and Spain is again the coldest while whole area between Sardinia and Corsica and Spain is warmer more then 3 degrees. Northern Adriatic and Ionian Sea together with central Mediterranean are slightly warmer then the rest, by about 2.2 degrees, while southern Adriatic is slightly cooler. Eastern Mediterranean stays at about 2.2-2.4 degrees warmer than for the present climate.

The global simulations have larger warming then CRCM in almost all inland regions of Spain, France, Italy, Balkans and Turkey. Differences are as large as 1.5-1.7 degrees. On the other hand, especially for DJF season Alps are less warmed, presumably due to the poorer horizontal resolution. The whole Mediterranean Sea has smaller increase in the SST.

Beside these main differences we have obvious differences in patterns due to differences in resolution. In comparison with the DJF season the SINTEXG simulation has now larger spatial variability and has less pronounced problems at the north-eastern corner which is understandable if the model has a bias there and that being removed in these differences.

4.3.2 THE PRECIPITATION FIELD

Next, in **Fig. 4.9**, we present differences in precipitation. Top left regional simulations for the DJF, and top right for the JJA season. The bottom panels have global results, for the winter to the left, and summer to the right. Fields are relative differences in accumulated precipitation in *percents*. For the DJF season, CRCM has almost every where *decrease* with variable amount, going from -50-0%. There is a small part of the domain, the south-center and the south-eastern part with increase between 10-40%. The largest differences are Saharan part of Algiers and Morocco. For the JJA season and land part of the domain, we have similar results with slightly larger decrease of precipitation over France and Northern Italy. Much larger are differences over the sea. Decrease in precipitation is from 10-50%, over the Mediterranean Sea but quite variable from region to region. The western Mediterranean, central and southern Adriatic show the largest decrease while central and eastern Mediterranean have increase of precipitation up to 40-50%. Similarly Algiers and Tunisia have increase in precipitation of 20-50% while north

and north-western parts of the domain have the smallest changes in both seasons. Very near Gibraltar, we get even larger decease of about 40-50 %.

The global simulations, for the DJF season, show quite different distribution of the differences in the precipitation filed. The north-western corner of the domain has increase from 20-40%. The same signal is in the south-eastern part of the domain over Aegean Sea, Turkey and western Mediterranean. At the Egypt-Israel border differences reach 50%. For the summer season we have large decrease almost everywhere. Over the Mediterranean decrease is from 70-90% with almost half of its area in the -90% range. Alps and Central Europe have weak increase, while Balkans has decrease of 30-40% in the northern part and almost 90% over Greece. Most of Italy, its central part has larger decrease of 70% with Sicily showing 90% decrease.

4.3.3 THE SURFACE WIND

In the end we present results of the 10m winds, but this time we present only its intensity. In **Fig. 4.9** we have, in the same order as before, on top the regional and bellow the global simulations. The DJF season has weak decrease over France and north-western part on the Mediterranean Sea. Over the Alboran Sea we have maximum increase which is almost 2m/s. The same increase is observed over Aegean Sea near the Turkish coast, few small areas in the southern Adriatic. Eastern half of the Mediterranean Sea has smaller increase in the wind speed in the range from 1-2 m/s. Near Eastern Adriatic coast we have decrease of about 0.5-1 m/s while inland of Balkans have weaker decrease.

For the JJA season regional simulations have weakening of the wind in the north-western corner over France and English channel .In the rest of the domain equally weak increase, slightly larger in the area of the Aegean Sea and Western Turkey, up to 1m/s.

Global simulations, for the DJF season, have in the whole western Mediterranean Sea decrease up to 1m/s and -0.5 ms/ in the rest of it. Similar to the regional simulations close to Gibraltar weakening is smaller then in the rest of the domain. Southern part of the land part of the domain from west to east has similar weak decrease while going to the north it turns into weak increase.

For the summer decrease of wind over Mediterranean Sea is now weaker, less than 0.5 m/s. Spain and France have increase from 0.5-1 m/s which is one of the two maximums. The other one is over Croatia and Hungary. In the rest of the domain signal is quite weak.

5. COMPARISON BETWEEN 20TH CENTURY (1961-1990) AND 21ST CENTURY A1B SCENARIO (2079-2100) WITH FOCUS ON ITALY AND SERBIA

In the end we will concentrate on the comparisons between the future climate and the present one for Italy and Balkans. Both Italy and Balkans show clear signal related to the future climate warming.

5.1 THE SURFACE TEMPERATURE

As shown in **Fig. 5.1**, for Italy, during the DJF season the strongest signal is in the northern part near the Alps. Alps themselves have the largest increase of the whole domain in the range 2.6-3.2 deg. For the rest of the northern Italy warming is up to 2.4 degrees. Central Italy facing the Adriatic shows smaller increase, about 2 degrees.

South and Sicily show about 1.6 degrees in warming. Northern Adriatic is warmer by 2-2.2 degrees as is Liguria Sea in the Gulf of Genoa. From the southern half of Sardinia a warm tongue of higher SST extends towards Calabria. The central and southern part of Adriatic is about 1.5 degrees warmer.

During the JJA season warming is more pronounced. The warm area over Alps has moved slightly to the south with much weaker gradients in comparison with the DJF season. Maximum of warming is still here and is about 3.6 degrees. The whole of the northern Italy shows similar warming about 3.4 with few spots of 3.8 degrees. Actually away from the coasts that warm belt extend thought the peninsula and is also visible in the Sicily. Only the coastal regions are cooler with warming about 3 degrees. Northern Adriatic is also warmer by almost 3 degrees and only in the south between Albania and Italy we have waters that are cooler with warming by 2.4 degree and a small spot with 2.2 degree. Sardinia is similar to the Sicily with 3.6 inland and less warming near the coast Both Tyrrhenian and Liguria Sea near the cost have warming by 1.6 but further to the west and around Sicily and Corsica it warms up to 3-3.2 degrees. The same stands for the Ionian Sea.

For the DJF season Serbia does exhibit warming as the rest of the domain but it is rather homogenous. Warming is in the range of 2-2.2 degrees. To the west of it signal is about .2 degrees stronger presumably due to the local orography there. For to the JJA season warming quite stronger, in the range 3.4-3.8 degrees. The warmer area is in the southern part of Vojvodina. The same signal is also present to the west in the Slavonia, region of Croatia. Probably the reason that larger variability over Italy then over Serbia is presence of the sea around Italy while the influence of the Adriatic over Serbia is subdued by the mountain range at the coast.

5.2 THE PRECIPITATION FIELD

For the DJF season we have decrease both for Italy and Serbia (**Fig. 5.2**). They are in the range of -50% to -10%. In the small are in the central Sicily we have even larger decrease of 70%. Even over surrounding seas of Italy we have similar situation.

For the JJA season we have quite different picture. Over Italy we have homogenous picture without variation between north and south. Alps have smaller decrease around 20% while the rest of Italy has decrease of about 50%. Only Sicily and sea around it has relative *increase* of almost 50%. Similar situation is for the island of Sardinia. On both sides of Italy, over seas, we have relative decrease of about 70%. The same signal is in coastal areas. Only northern Adriatic has relative decrease of about 50%.

On the contrary the Serbian region has quite homogenous distribution, with small relative decease of about 20%, with few small areas of even smaller relative decrease close to 10%.

5.3 DISTRIBUTIONS OF TEMPERATURE AND PRECIPITATION

Besides just showing if the future climate is warmer and if so how much we are interested into possible variability of the future climate within the time slice. A partial answer to that question can be given by calculating mean annual distribution of temperature and precipitation. These distributions are presented in **Fig. 5.3a** for temperature and **Fig. 5.3b** for the precipitation. These distributions are for Italy only. On horizontal axes data is grouped or binned into classes of one degree. Distributions show number years belonging to a certain bin out of total of number of bins, spanning the time slice interval of 30 years. So for instance green line on the first, left panel in **Fig. 5.3a**, has maximum of 12 years for the bin 1-2 degrees which means that in abut 12 years out of 30 mean T_{2m}, for the DJF season will be between 1 and 2 degree. These distributions where calculated for three regions north, central and south and for two different seasons. In all T_{2m} graphs we see the shift towards higher temperatures. For the DFJ season and for the north part of the country number of warmest years slightly increases from about 12 to about 15 with increase in T2m from bin 1-2 degrees to bin 3-4 degrees. For the JJA season the shift is from 20-21 to 23-25 degrees which means that distribution is wider with reduced maximum from about 13 years to 10 years.

For the central region and for the DJF season future distribution gets narrower with slight increase of maximum by about a year. The JJA season show significant shit toward larger temperatures while becoming more symmetric around to the maximum. Finally for the south region during the DJF season shift is towards higher temperatures is from 6-7 to 8-9 degrees. Number of years to the left of maximum increases while it decreases on the other side of the maximum. JJA season has pronounced local maximum in the 26-27 bin, narrower than either the north nor in the central region.

In **Fig. 5.3b** we present the precipitation distributions with abscissa showing monthly accumulation of precipitation in mm/month. For the precipitation in most of the seasons and regions the shift is towards reduction of the precipitation. The DJF season, for all regions, is the season with larger amount of precipitation and that stays for the future to. In the north, for the DJF season maximum slightly increases with reduction of instances with heavier precipitation. The JJA season shifts from relatively flat distribution towards distribution with maximum for the weak and medium rains and very small for values for the heavier rains. Similar goes for the central region in both seasons. South region in the DJF season shifts to the left, towards weaker precipitation, from about 25 mm/month to about 15 mm/month with decrease in value of the maximum. For the JJA total amount of precipitation stays roughly the same but is shifted towards weaker rains. Maximum of occurrence is 0-2.5 mm/month.

6. PARAMETRIZATION OF CONVECTION

Among the most important components of any model to be used for climate simulations are its moist parameterizations, both for deep and shallow convection. Most of the existing convection schemes are either of the adjustment type or mass flux type. Present scheme in the SINTEXG model, designed by Tiedtke (1983, 1989, 1993, Tid in the further text) belongs to the mass flux type class of schemes. Task 3, of the SINTA project, was to implement another cumulus scheme, Betts-Miller-Janjić (1986 I, II, 1990, 1994, BMJ in the further text) cumulus scheme and compare its performance with the one from the existing cumulus scheme.

6.1 BETTS-MILLER-JANJIĆ CUMULUS SCHEME, BRIEF SUMMARY

The BMJ cumulus scheme has been originally developed by Betts and Miller and got its present form by Z. Janjić. The BMJ scheme belongs to the adjustment class of schemes. The basic idea is that during a convective episode a vertical profile of temperature and humidity approach reference profile that can be specified. The form of the adjustment in the original (Betts-Miller, 1986) was:

$$\frac{\partial T}{\partial t} = -\frac{T - T_{ref}}{\tau},$$

$$\frac{\partial Q}{\partial t} = -\frac{Q - Q_{ref}}{\tau},$$

where τ is a constant, time scale of the duration of the convection episode. After implementation of BMJ scheme in the operational model of NCEP it was discovered that occasionally scheme has tendency to produce excessive precipitation in isolated points even to the degree that forecast could into be finished.

After extensive analysis Janjić traced the problem to several components of the original scheme, regarding construction of the reference profiles and value of the time constant τ. Instead of being constant, he introduces cloud efficiency as a new variable and makes τ a function of it. Basically cloud efficiency measures how far away temperature profile from being isentropic is. The closer its gets to the isentropic the longer τ should be. In that way excessive rains were eliminated and better over all scores made. For more details about the scheme see the appendix. In order to make "clean" comparison of the two schemes the BMJ scheme was implemented in the same routine that calculates the convective heating in the SINTEXG model, in the *cudtdq* module. Logical switch *lo_bmj* activates one or the other cumulus scheme. Convective heating and moistening are then stored in the 3 dimensional fields *dtdt-bmj* and *dtdq-bmj*. They are added to the SINTEXG fields *ptte* and *pqte* that carry updates from all physical processes.

The results are presented as latitude-longitude dependent fields of vertically integrated convective heating, converted in the amount of precipitation. Since it is traditional to present convective heating through zonal averages at the end we have done that too.

6.2 RESULTS

We present results for the integration whose length was four months starting with the January, with standard climatological initial fields for that particular horizontal and vertical resolution. We present results from the horizontal resolution was T106 meaning 106x180 in longitude, latitude and 19 vertical levels, although during the testing period all lower resolutions were run as well (T30, T41 and T63).

The numbers that are presented start with cumulus precipitation, accumulated over 24 hours (after that the "bucket" was emptied), the standard period of precipitation accumulations especially if we want to make comparisons with measured precipitation. These accumulations were further averaged over one month and results are given in **Figs. 6.1a,b,c** for three consecutive months. The left row of panels has precipitation calculated using the Tid scheme while the right row is for the BMJ scheme. At the first glance there is a general agreement between the two schemes which can serve as a rough check of the implementation of the BMJ scheme. Closer examination shows differences between the two schemes. The largest difference is presence/absence of the areas with weak precipitation. Such areas are present in runs with the Tid scheme in several places of the world, the Pacific Ocean to the north of the equator, coloured in purple, that extends all the way to the North America coast, to the south of the equator, the north-east Africa, and eastern Mediterranean region.

Over Arabian Sea and Indian subcontinent we have weak precipitation in both runs but it is more pronounced in the case of the Tid scheme. Similar conclusions stand for South America. In the south Pacific there is large such zone in Tid case while in the BMJ case it is barely visible. In the case the south Atlantic, of the Argentinean coast we have the opposite, BMJ produces wider weak precipitation zone. The second difference is in the areas that have more intense precipitation. Now the BMJ scheme produces more such areas. The most pronounced regions are south of the equator, near Australia to the east of it, the Caribbean region and eastern Mediterranean region. First we note that zones of the precipitation stay in one position throughout the integration. One such instance is the Amazon area in Brazil. For the Tid scheme rain slightly intensifies but stays fixed over the land. In the BMJ runs it is shifted to the east, over the ocean and is more efficient, relative to the Tid run, in producing the rain.

Beside these latitude-longitude fields we show zonal averages of the monthly means thus creating South-North profiles. These profiles are presented in **Fig. 6.2**.

Blue curves are for the standard, Tid, cumulus scheme while red curves are for the new, BMJ, scheme. Again as in the previous figure there is general agreement between two schemes. Both schemes have double maximum to the north and south of the equator. The BMJ scheme has larger precipitations in the Equatorial region then Tid scheme and more pronounced to the south of the Equator. To the North of the Equator we have similar result although less pronounced. This means that the BMJ alone is not able to rectify the known deficiency of the SINTEXG model that puts the ITCZ to the south of the Equator instead of its proper position slightly to the north of the Equator.

The BMJ cumulus scheme has been successfully implemented into the SINTAXG global model. In comparison with the original, Tid, scheme precipitations patterns are similar with less areas of weak precipitation. Patterns of the areas with are more often present in the runs with the BMJ scheme and are more in the form of discontinuous patches. Zonal averaged profiles show that even more clearly. Problem of the positioning of the ITCZ stays as in the original cumulus parameterization.

7. CONCLUSIONS

The climate of the Euro-Mediterranean region and the main features of its variability are evaluated by means of a global climate model and a regional climate model; the models results are also compared to observational data sets. In addiction both models, after some preliminary simulations with increasing greenhouse gases (GHGs) concentrations, have been used to simulate the possible climate changes induced by GHGs and sulphate aerosols in the 21st century by applying the climate scenario *A1B* from IPCC. The main scientific conclusions regarding the possible climate change at the end of the 21st century:

1) **The global climate simulation for the end of the 21st century:**

- The warming is largest over the north-eastern from autumn to spring, whereas during boreal summer, the largest warming is located over southern Europe and in the Mediterranean region, where it appears to exceed 5°C.

- On the other hand, the precipitation appears to increase over northern Europe and decrease over the southern Europe and the Mediterranean region. In boreal spring and summer, most of the Euro-Mediterranean is characterized by a decrease of precipitation in the *A1B* simulation, with a slight increase mostly confined at very high latitudes (northern than 60°N).

- Therefore, according the *A1B* scenario, the southern part of Europe and the Mediterranean region during the late part of the 21st century could be characterized by a substantially hotter climate during summer and drier conditions, particularly intense during the autumn and winter seasons. In some part of the Iberian Peninsula, Alpine region, Italy and on the western Balkans, the reduction of rainfall might be considerably strong, larger than 1 mm/day, which represents a depletion of about 20% of the mean precipitation found during the 1961-1990 period. These findings are fully consistent with the results obtained with numerous other models (e.g., IPCC-AR4 2007) and thus they appear to be very robust.

2) **The regional climate simulation for the end of the 21st century:**

- Projected changes of the surface air temperature, due to the increase in GHGs, are in between 1.2-3.5°C for the winter season, while are larger and in the range 1.8-4.2°C for the summer season. Locally larger values are connected either to the local topography, Alps, Pyrenees, Balkan Mountains, and Apennines or to both topography and land-sea line (Italy case). For Balkans the projected surface air temperature changes are between 2.0-2.4°C, while for Italy the changes are between 1.8-2.4°C. Projections for the summer season show larger increase, with 3.4-3.8°C for Serbia and 3.2-4.0°C for Italy.

- Projected changes of the precipitation for the winter season show almost everywhere decrease with variable amount, going from -50 to 0%. There is a small part of the domain, north-east Africa, with increase between 10 and 40%, and also north-east part of east Europe with 0-10% increase of precipitation. During summer season decrease again appear over almost whole model domain, even with some areas with values greater of 70%. This maximum of summer decrease can be found along costal zones (especially Italian costal area) with values up to 70%.

- Projected changes for the surface winds show weak decrease over France and north-western part on the Mediterranean Sea. Near eastern Adriatic coasts the surface winds shows a decrease of about 0.5-1.0 m/s while the show a weaker decrease inland of Balkans. For the summer season, decrease of surface winds is weaker over Mediterranean Sea, less than 0.5 m/s. On the other hand, Spain and France show an increase of surface winds (0.5-1.0 m/s) along with Croatia and Hungary. In the rest of the domain signal is quite weak.

- Summarizing, the results from the climate regional model for the end of 21st century, following *A1B* scenario, show overall increase in surface air temperature and decrease in precipitation over the Euro-Mediterranean region. High increase in surface air temperature has been found during summer season (June-July-August), close to 4°C, over both Italy and Serbia. Decrease in precipitation is also amplified during summer season with maximum over Italian costal zone. In some areas the decrease of precipitation is about 70% respect to 1961-1990 period. Changes of surface wind magnitude shows much complicated structure, changing sign from season to season and from area to area. As for global model these results are in agreement with results obtained with other regional climate models (e.g., IPCC-AR4 2007, Chapter 11, Regional Climate Projections).

- **Finally, this project has confirmed that using an advanced high resolution global climate model along with an advanced high resolution regional climate model connected through dynamical downscaling is a successful approach in order to capture many small-scale processes in the atmosphere and the ocean. This is due to better representation (more detailed structure) of some characteristics of climate system (topography, soil and vegetation types, land-sea coastline, etc.).**

- **These high resolutions climate data can be used for climate change impact models of the Italian and Serbian areas in order to investigate small-scale phenomena, like sediment transport in coastal areas, hydrological cycles over smaller river basins and hydropower production.**

REFERENCES

Arakawa, A., and V. Lamb (1977), Computational design of the basic dynamical processes of the UCLA general circulation model. in Methods in Computational Physics, Vol. 17, pp. 174–265, Academic Press.

Baldwin, M.E., and T.L. Black, 1996: Precipitation forecasting experiments in the western U.S. with NCEP's mesoscale Eta model. Preprints, 11th Conf. on Num. Wea. Pred., AMS, Norfolk, VA. Aug, 1996

Behera S.K., J.J. Luo JJ, S. Masson, P. Delecluse, S. Gualdi, A. Navarra, T. Yamagata, 2005: Paramount impact of the Indian Ocean dipole on the East African short rains: A CGCM study. {\it J. of Clim.}, {\bf 18}, 4514--4530.

Betts, A.K., 1986: A new convective adjustment scheme. Part I: Observational and theoretical basis. Quart. J. Roy. Meteor. Soc., 112, 677-691.

Betts, A.K., and M.J. Miller, 1986: A new convective adjustment scheme. Part II: Single column tests using GATE wave, BOMEX, and arctic air-mass data sets. Quart. J. Roy. Meteor. Soc., 112, 693-709.

Blanke B., P. Delecluse, 1993: Low frequency variability of the tropical Atlantic ocean simulated by a general circulation model with mixed layer physics. {\it J. Phys. Oceanogr.}, {\bf 23}, 1363--1388.

Blanke B., P. Delecluse, 1993: Low frequency variability of the tropical Atlantic ocean simulated by a general circulation model with mixed layer physics. {\it J. Phys. Oceanogr.}, {\bf 23}, 1363--1388.

Blumberg, A., and G. Mellor (1987), Description of a three-dimensional coastal ocean circulation model., in Three-Dimensional Coastal Ocean Models, 4, edited by N. Heaps, p. 208p, American Geophysical Union, Washington, DC.

Brasseur, P., Brankart, J-M., Shomnenauen, R. and Beckers, J-M, 1996,

Seasonal Temperature and Salinity Fields in the Mediterranean Sea : Climatological Analyses of an Historical Data Set, 43, deep sea research, 159-192,

Carlos Pérez, Slobodan Ničković, Goran Pejanović , José María Baldasano and Emin Özsoy ,2006: Interactive dust-radiation modeling: A step to improve weather forecasts Journal of Geophysical Research,, VOL. 111, D16206, doi:10.1029/2005JD006717, 2006

Ekman AML, Rodhe H (2003) Regional temperature response due to indirect sulfate aerosol forcing: impact of model resolution. Clim Dynam 21:1–10

Fels, S. B., and M. D. Schwarzkopf (1975), The simplified exchange approximation: A new method for radiative transfer calculations, J,of the Atm. Sci., 32, 1475–1488.

Giorgi, F., X. Bi , J. S. Pa, 2004:I Mean, interannual variability and trends in a regional climate change experiment over Europe. I. Present-day climate (1961–1990) Climate Dynamics (2004) 22: 733–756

Giorgi, F., Xi Xunqiang Bi , Jeremy Pal, 2004: Mean, interannual variability and trends in a regional climate change experiment over Europe. II: climate change scenarios (2071–2100), Climate Dynamics (2004) 23: 839–858

Giorgi. F. and M.R. Marimicci. 1996a: An investigation of the sensitivity of simulated precipitation to model resolution and its implications for climate studies. Man. Wea. rev., 124, 118-166.

Giorgi F. and M.R. Marinucci, 1996b: Improvements in the simulation of surface climatology over the European region with a nested modeling system. Geophysical Research Letters, 23. 27:3 276.

Giorgi. F.. 1995: Perspectives for regional earth system modeling. Global and Planetary Change, 10, 23-42.

Giorgi. F., C. Shields Brodeur. and G.T. Bates. 1994: Regional climate change scenarios over the United States produced with a nested regional climate model. Journal of Climate, 7, 375-399.

Giorgi. F.. M.R. Marinucci, and G.T. Bates. 1993a: Development of a second generation regional climate model (REGCM2). Part I: Boundary layer and radiative transfer processes. Monthly Weather Review, 121. 2794-2813.

Giorgi. F., M.R. Marinucci, G. De Canio and G.T. Bates, 1993b: Development of a second generation regional climate model (R.EGCM2). Part TT: Cumulus cloud and assimilation of lateral boundary conditions. Monthly Weather Review. 121, 2811-2832.

Giorgi. F.. and L.O. Mearns, 1991: Approaches to regional climate change simulation: A review. Reviews of Geophysics, 29, 191-216.

Giorgi. F., and M.R. Marimicci. 1991: Validation of a regional atmospheric model over Europe: Sensitivity of wintertime and summertime simulations to selected physics parameteriza.tions and lower boundary conditions. Quarterly Journal, of the Royal Meteorological Society, 117, 1171-1207. 27

Giorgi. F., 1990: On the simulation of regional climate using a limited area modelnested in a general circulation model. Journal of Climate., 3, 941 963.

Giorgi. F.. M.R. Marinucci, and G. Visconti, 1990: Use of a limited area model nested in a general circulation model for regional climate simulation over Europe. Journal of Geophysical Research, 95. 18,413 18.4:31.

Giorgi. F., and G. T. Bates, 1989: On the climatological skill of a regional model over complex terrain. Monthly Weather Review, 117; 2325-23-17.

Gualdi, S., A. Navarra, E. Guilyardi, and P. Delecluse, 2003a: Assessment of the tropical Indo-Pacific climate in the SINTEX CGCM, {\it Ann. Geophysics}, {\bf 46}, 1--26.

Gualdi, S., E. Guilyardi, A. Navarra, S. Masina, and P. Delecluse, 2003b: The interannual variability in the tropical Indian Ocean as simulated by a CGCM. {\it Clim. Dyn.}, {\bf 20}, 567--582.

Guilyardi, E., P. Delecluse, S. Gualdi, and A. Navarra, 2003: Mechanisms for ENSO phase change in a coupled GCM, {\it J. of Clim.}, {\bf 16}, 1141--1158.

Huntingford, C., R. G. Jones, C. Prudhomme, R. Lamb and J. H. C. Gash, 2003: Regional climate model predictions of extreme rainfall for a changing climate. Q. J. R. Meteorol. Soc. 129:1607-1621

Janjic, Z. I. (1996), The surface layer parameterization in NCEP Eta model, pp. 4.16–4.17, WMO, Geneva, CAS/C WGNE, 4.16-4.17.

Janjić, Z.I.,(1994), The step-mountain eta coordinate model: Further developments of the convection, viscous sub-layer, and turbulence closure schemes. Mon. Wea. Rev., 122, 927-945

Janjić, Z. I. (1990), Physical package for step-mountain, eta coordinate model., Mon. 272 Wea. Rev., 118, 1429–1443.

Janjić, Z. (1984), Non-linear advection schemes and energy cascade on semistaggered grids, Mon. Wea. Rev., 112, 1234–1245.

Janjić, Z. I. (1979), Forward-backward scheme modified to prevent two-grid-interval noise and its application in sigma coordinate models., Contrib. Atmos. Phys., 52, 69–84.

Janjić, Z. I. (1977), Pressure gradient force and advection scheme used for forecasting with steep and small scale topography., Contrib. Atmos. Phys.,, 50, 186–199.

Jones, P.D., D.E. Parker, T.J. Osborn, and K.R. Briffa. 2006: Global and hemispheric temperature anomalies--land and marine instrumental records. In Trends: A Compendium of Data on Global Change. Carbon Dioxide Information Analysis Center, Oak Ridge National Laboratory, U.S. Department of Energy, Oak Ridge, Tenn., U.S.A.

Jones RG, Murphy JM, Noguer M, Keen M (1997) Simulation of climate change over Europe using a nested regional climate model. I: comparison of driving and regional model responses to a doubling of carbon dioxide. Q J R Meteorol Soc 123:265–292

Kuo, H.-L., 1974: Further studies of the parameterization of the influence of cumulus convection on large-scale flow. J. Atmos. Sci., 31, 1232-1240.

Kalnay et al., The NCEP/NCAR 40-year reanalysis project, Bull. Amer. Meteor. Soc., 77, 437-470, 1996.

Lazić, L., 1993: Eta model forecasts of tropical cyclones from Australian Monsoon Experiment: The model sensitivity. Meteorol. Atmos. Phys., 52, 113-127

Luo, J.-J., S. Masson, S. Behera, P. Delecluse, S. Gualdi, A. Navarra, and T. Yamagata, 2003: South Pacific origin of the decadal ENSO-like variation as simulated by a coupled GCM. Geop[hys. Res. Lett., 30, 2250, doi:10.1029/2003GL018649.

Madec, G., P. Delecluse, M. Imbard, and C. Levy, 1999: OPA 8.1 Ocean General Circulation Model reference manual, Internal Rep. 11, Inst. Pierre--Simon Laplace, Paris, France.

Masson S., Impact of barrier layer on winter--spring variability of the southeastern Arabian Sea. {\it Geophys. Res. Lett.}, 32, L07703, doi:10.1029/2004GL021980.

Mesinger, F., 1984: A blocking technique for representation of mountains in atmospheric models. Riv. Meteor. Aeronaut., 44, 195-202

Mesinger, F., Z. Janjić, S. Nicković, D. Gavrilov, and D. Daven (1988), The step mountain coordinate: model description and performance for cases of alpine lee cyclogenesis and for a case of an Appalachian redevelopment, Mon. Wea. Rev., 116, 1493–1518.

Mellor, G., and T. Yamada (1974), A hierarchy of turbulence closure models for the planetary boundary layer, J. Atmos. Sci., 31, 1791–1806.

Mellor, G. L., and T. Yamada (1982.), Development of a turbulence closure model for geophysical problems., Rev. Geophys and Space Phys., 20(4), 851–875.

Mellor, G. L. (Ed.) (2002), Users guide for a three-dimensional, primitive equation, numerical ocean model, Program in Atmospheric and Oceanic Sciences, Princeton University, Princeton, NJ 08544-0710.

Mocrette J.J., 1991: Radiation and cloud radiative properties in the European centre for medium range weather forecasts forecasting system. J. Geophys. Res., 96, 9121--9132.

New, M., Hulme, M. and Jones, P.D., 1999: Representing twentieth century space-time climate variability. Part 1: development of a 1961-90 means monthly terrestrial climatology. Journal of Climate 12, 829-856

New, M., Hulme, M. and Jones, P.D., 2000: Representing twentieth century space-time climate variability. Part 2: development of 1901-96 monthly grids of terrestrial surface climate. Journal of Climate 13, 2217-2238

New, M., Lister, D., Hulme, M. and Makin, I., 2002: A high-resolution data set of surface climate over global land areas. Climate Research 21

Nordeng T.E., 1994: Extended versions of the convective parametrization scheme at ECMWF and their impact on the mean and transient activity of the model in the Tropics. ECMWF Research Department, Technical Memorandum No. 206, October 1994, European Centre for Medium Range Weather Forecasts, Reading, UK, 41 pp.

Räisänen J, Hansson U, Ullerstig A, Döscher R, Graham LP, Jones C, Meier HEM, Samuelsson P, Willen U, (2004), European climate in the late twenty-.rst century: regional simulations with two driving global models and two forcing scenarios. Clim Dynam 22:13–31

Roeckner E, and Coauthors (1996) The atmospheric general circulation model Echam-4: model description and simulation of present-day climate. Max-Planck-Institut fur Meteorologie, Rep. No 218, Hamburg, Germany, 90 pp.

Ronald B, Stull 1988: Introduction to Boundary Layer Meteorology, Kluwer Academic Pub., **ISBN:** 9027727686

Tiedtke, M., 1983: The sensitivity of the time-mean large-scale flow to cumulus convection in the ECMWF model. ECMWF Workshop on Convection in large-scale Models, 28 Nov.-1 Dec. 1983, Reading, England, 297-316.

Tiedtke M., 1989: A comprehensive mass flux scheme for cumulus parametrization in large--scale models. Mon. Weather Rev., 117, 1779--1800.

Tiedtke, M, 1993: Representation of clouds in large-scale models. Mon. Wea. Rev., 121, 3040-3061.

Timmermann R., H. Goosse, G. Madec, T. Fichefet, C Ethe and V. Duliere, On the representation of high latitude processes in the ORCALIM global coupled sea ice-ocean model, Ocean Modell., 8, 175-201, 2005. Winninghoff., F. J. (1968), On the adjustment toward the geostrophic balance in a simple primitive equation model with application to the problems of initialization and objective analysis., Ph.D. Thesis, UCLA.

Willmott CJ, Matsuura K (2001) Terrestrial air temperature and precipitation: monthly and annual time series (1950–1999) (version 1.02). Center for Climate Research University of Delaware, Newark, N.J., USA

Winninghoff., F. J. (1968), On the adjustment toward the geostrophic balance in a simple primitive equation model with application to the problems of initialization and objective analysis., Ph.D. Thesis, UCLA.

Winninghoff., F. J. (1968), On the adjustment toward the geostrophic balance in a simple primitive equation model with application to the problems of initialization and objective analysis., Ph.D. Thesis, UCLA.

Y. Kurihara “A Scheme of Moist Convective Adjustment” Monthly Weather Review, Vol. 101, No. 7, Jul. 1973, pp. 547-553

FIGURES:

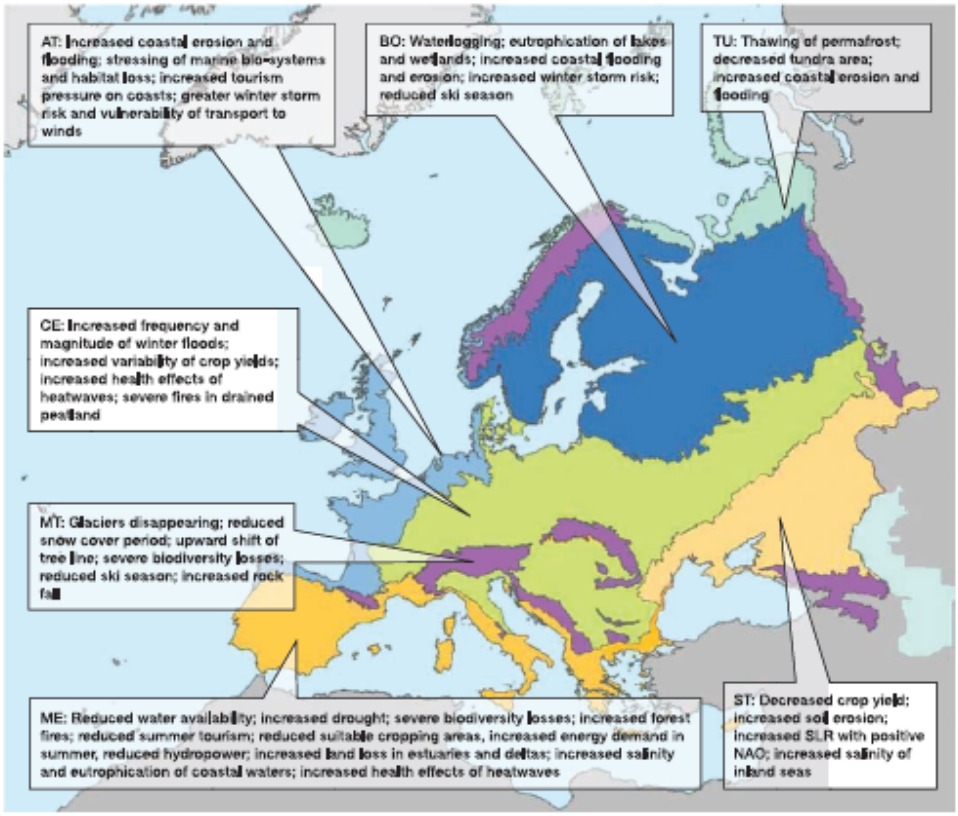

Fig. 1.1: Key vulnerabilities of European systems and sectors to climate change during the 21st century for the main bio-geographic regions of Europe (EEA, 2004): *(Source: Figure 12.3 – Alcamo et al., 2007: Europe. Climate Change 2007: Impacts, Adaptation and Vulnerability. Contribution of Working Group II to the Fourth Assessment Report of the Intergovernmental Panel on Climate Change, M.L. Parry, et al., Eds., Cambridge University Press, Cambridge, UK, 541-580)*

Sectors and Systems	Impact	Area				
		North	Atlantic	Central	Mediterr.	East
Water resources	Floods	↓↓	↓↓	↓↓	↓	↓↓↓
	Water availability	↑↑	↑↑	↓	↓↓↓	↓↓
	Water stress	↑↑	↑↑	↓	↓↓↓	↓↓
Forest, shrublands and grasslands	Forest NPP	↑↑↑	↑↑	↑ to ↓	↓	↑ to ↓
	Northward/inland shift of tree species	↑↑↑	↑↑	↑↑	↑ to ↓	↓↓
	Stability of forest ecosystems	↓↓	↓	↓	↓↓↓	↓↓↓
	Shrublands NPP	↑↑↑	↑↑↑	↑	↓↓↓	↓↓
	Natural disturbances (e.g., fire, pests, wind-storm)	↓	↓	↓	↓↓↓	↓↓
	Grasslands NPP	↑↑↑	↑↑	↑ to ↓	↓↓↓	↑
Biodiversity	Plants	↓↓	↓↓	↓↓↓(Mt)	↓↓↓	↓
	Amphibians	↓↓	↓↓↓	↑↑	↓↓↓(SW) ↑↑(SE)	↑↑↑
	Reptiles	↓↓	↓↓	↑↑	↓↓↓(SW) ↑↑↑(SE)	↑↑↑
	Marine mammals	↓↓↓	??	na	↓↓↓	??
	Low-lying coastal birds	↓↓↓	↓↓↓	na	↓↓↓	??
	Freshwater biodiversity	↑ to ↓	??	??	↓↓↓	??
Agriculture and fisheries	Suitable cropping area	↑↑↑	↑↑	↑	↓↓	↓
	Agricultural land area	↓↓	↓↓	↓↓	↓↓	↓↓
	Summer crops (maize, sunflower)	↑↑↑	↑↑	↑	↓↓↓	↓↓
	Winter crops (winter wheat)	↑↑↑	↑↑	↑ to ↓	↓↓	↑
	Irrigation needs	na	↑ to ↓	↓↓	↓↓↓	↓
	Energy crops	↑↑↑	↑↑	↑	↓↓	↓
	Livestock	↑ to ↓	↓	↓↓	↓↓	↓↓
	Marine fisheries	↑↑	↑	na	↓	na
Energy and transport	Energy supply and distribution	↑	↑↑	↑	↓	↑
	Winter energy demand	↑↑	↑↑	↑	↑↑	↑
	Summer energy demand	↓	↓	↓↓	↓↓↓	↓↓
	Transport	↑	↓	↓	↓	↑
Tourism	Winter (including ski) tourism	↑↑	↓	↓↓↓	↑↑↑	↓↓
	Summer tourism	↑	↑↑	↑	↓↓	↑
Property insurance	Flooding claims	??	↓↓	↓↓	??	??
	Storms claims	↓	↓↓	↓↓	??	??
Human health	Heat-related mortality/morbidity	↓	↓↓	↓↓	↓↓↓	↓↓
	Cold-related mortality/morbidity	↑	↑↑	↑↑	↑	↑↑↑
	Health effects of flooding	↓	↓↓	↓↓	↓↓	↓↓
	Vector-borne diseases	↓	↓	↓	↓↓	↓↓
	Food safety/Water-borne diseases	↓	↓	↓	↓↓	↓↓
	Atopic diseases, due to aeroallergens	↓	↓	↓	↓	↓

Table 1.1:. *Summary of the main expected impacts of climate change in Europe during the 21st century, assuming no adaptation. (IPCC-AR4-WGII) (Source: based on* Table 12.4 *- Chapter 12 Europe – Alcamo et al., 2007: Europe. Climate Change 2007: Impacts, Adaptation and Vulnerability. Contribution of Working Group II to the Fourth Assessment Report of the Intergovernmental Panel on Climate Change, M.L. Parry, et al., Eds., Cambridge University Press, Cambridge, UK, 541-580)*

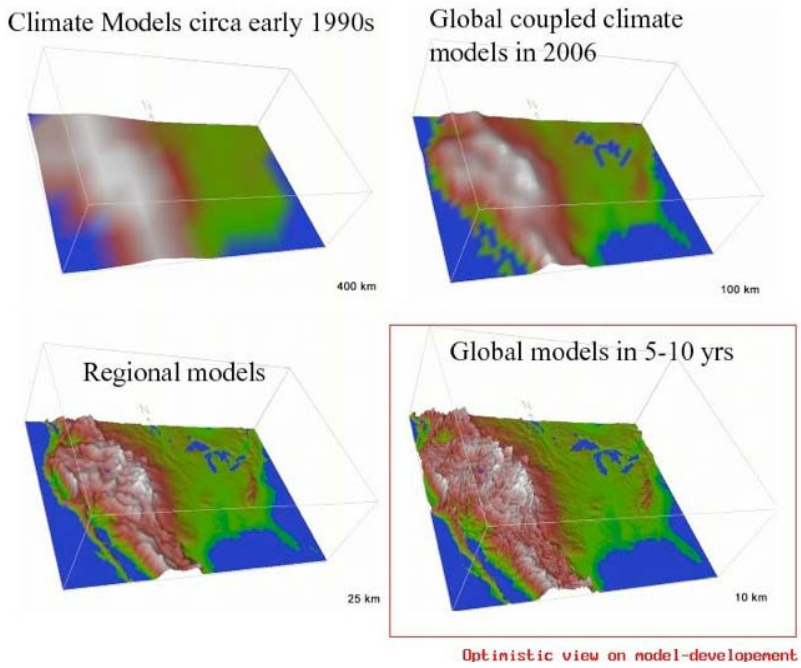

Fig. 1.2: Representation of the topography with different horizontal resolutions. Top left for the 400 km grid, top right 100 km grid, bottom left 25 km grid, resolution of CRCMs and bottom left 10 km grid (Source: *http://www.realclimate.org/index.php/archives/2007/05/climate-models-local-climate/*)

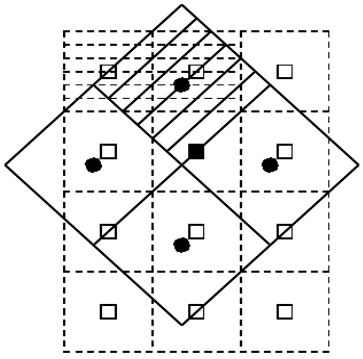

Fig. 2.1: Overlap of the land and sea masks. Diamond represents four grid points of the atmospheric model, denoted by the filled circles. Rectangular, in dashed lines, represents twelve grid points of the ocean model, denoted with empty squares. Top grid point of the atmospheric model is a land point. Two, top and left points, in dashed lines, are land points of the ocean model. Filled square, a water point for the ocean model is a land point for the atmospheric model.

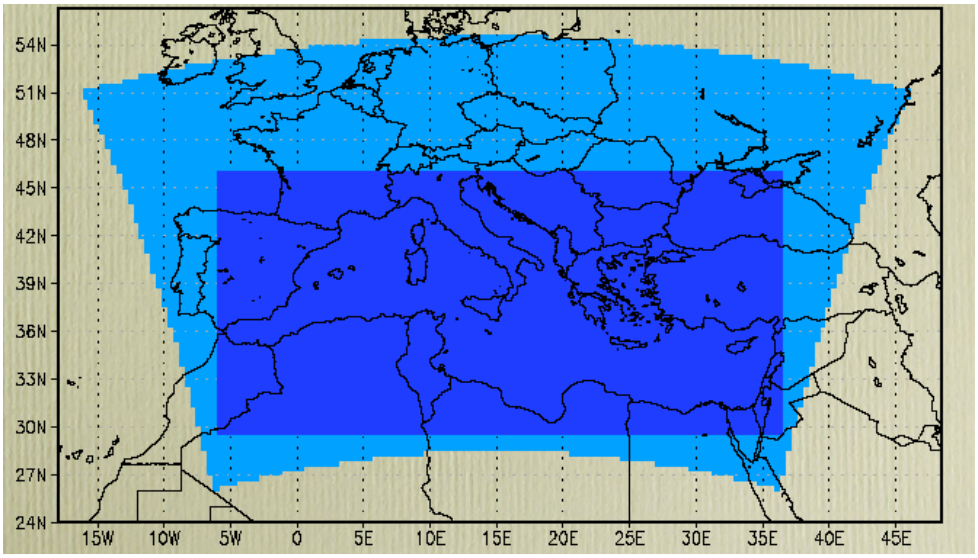

Fig. 2.2: Relative positions of the both model, with atmospheric model domain (Eta) light blue and the POM domain dark blue.

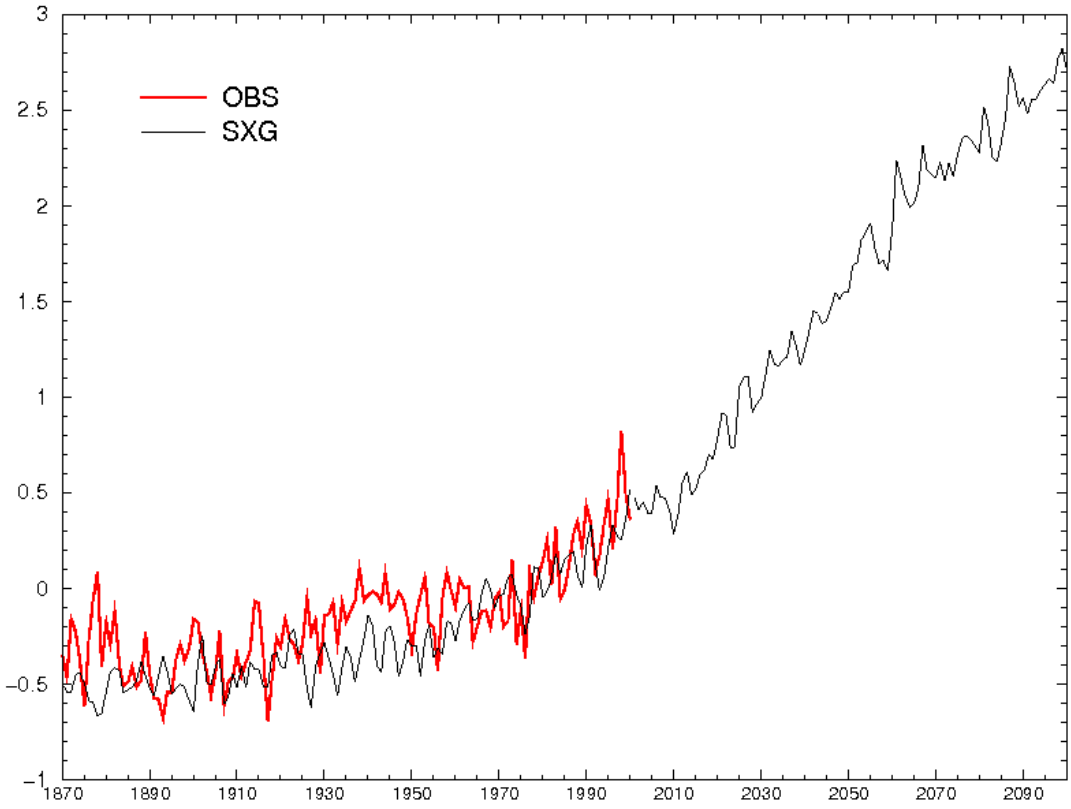

Fig. 3.1: Time series of the annual mean values of surface temperature averaged over the entire globe. The values plotted are the year-to-year deviation with respect to the 1870-1890 mean. The red line is the observations; the black line is the model integration (1870-2000, 20C simulation; 2001-2100 A1B scenario simulation)

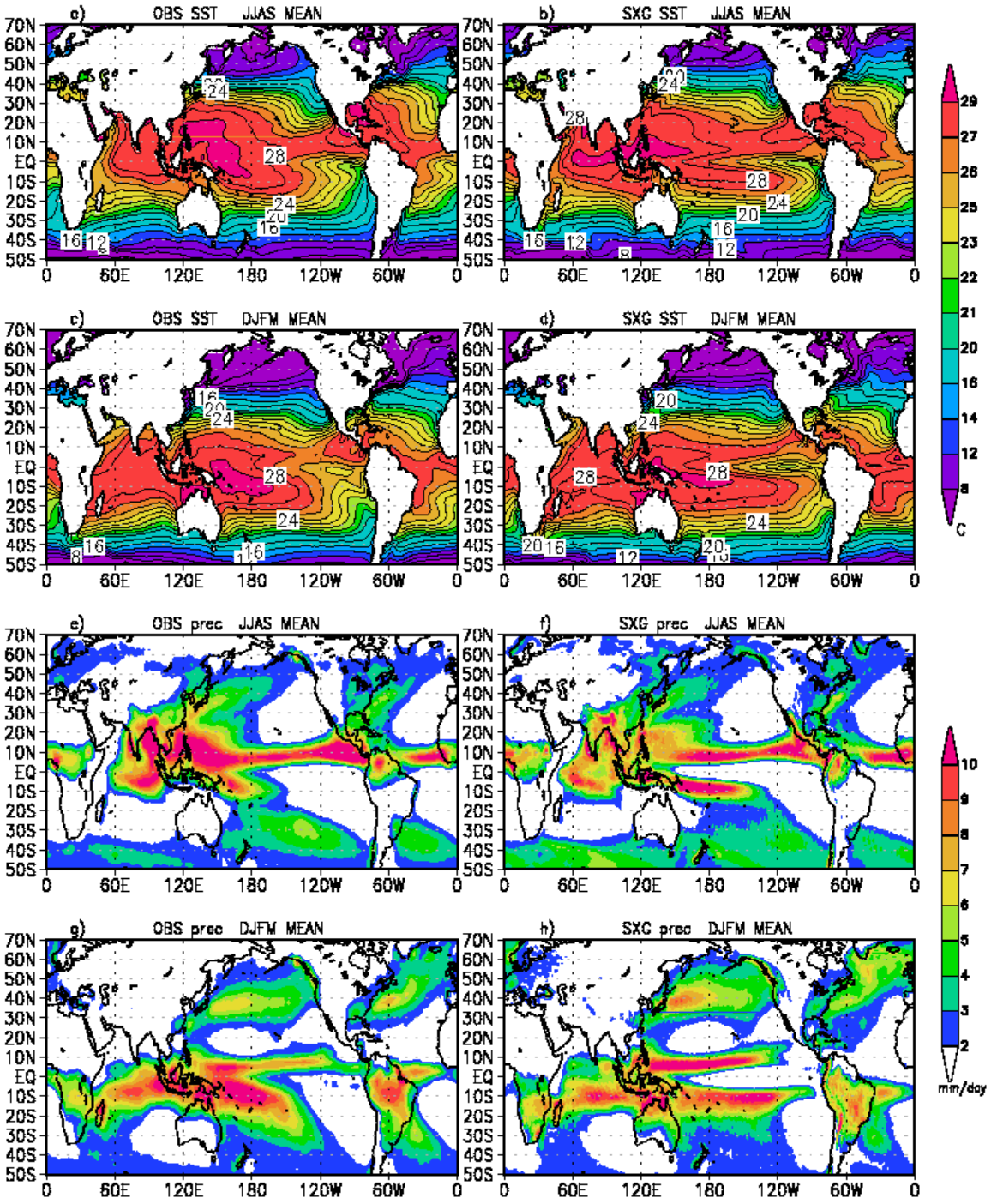

Fig. 3.2: Seasonal means, northern winter (December-March, DJFM) and northern summer (June-September, JJAS), of sea-surface temperature (SST, expressed in °C), upper panels, and precipitation (in mm/day), lower panels. In the left column are the mean field obtained from the observations and in the right panels are the mean fields obtained from the 20C simulation. Both for the observations and the model the seasonal means have been computed for the period 1961-1990.

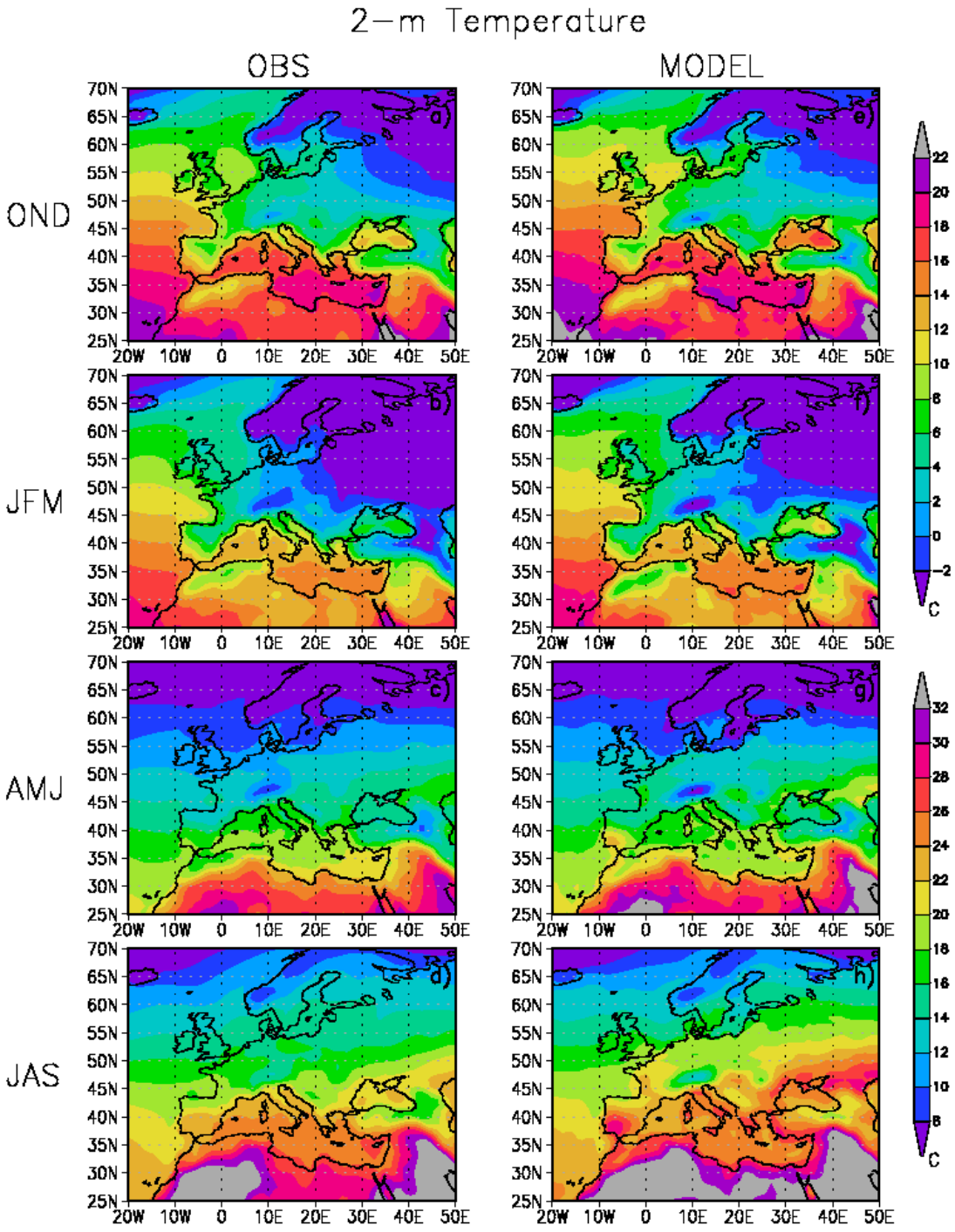

Fig. 3.3: Seasonal means of the 2-metres temperature (T2m) during the period 1961-1990 obtained from the ERA-40 (left panels) and the 20C simulation (right panels). In order to emphasize the regional characteristics of the seasonal cycle, the mean northern autumn (October-December, OND), northern winter (January-March, JFM), northern spring (April-June, AMJ) and northern summer (July-September, JAS) are shown. The contour shading is 2°C and for the northern autumn and winter the contour range is from -2°C to 22°C, whereas for northern spring and summer, the contour range is from 8°C to 32°C.

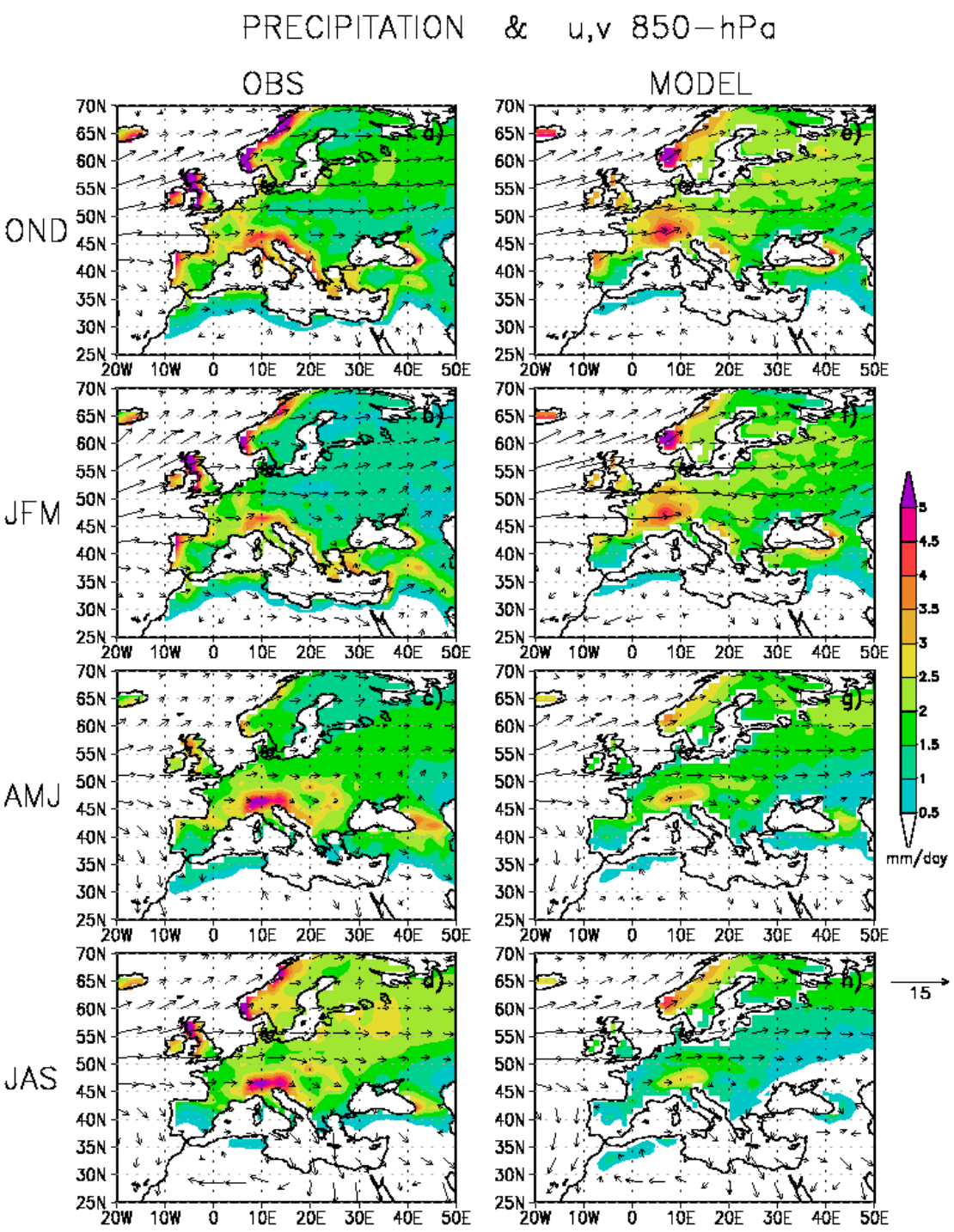

Fig. 3.4: As in Figure 3.3 but for seasonal means of precipitation (shaded patterns) and 850-hPa wind velocity (arrows). Shading contour is 0.5 mm/day. Arrow length scale is 15 m/s.

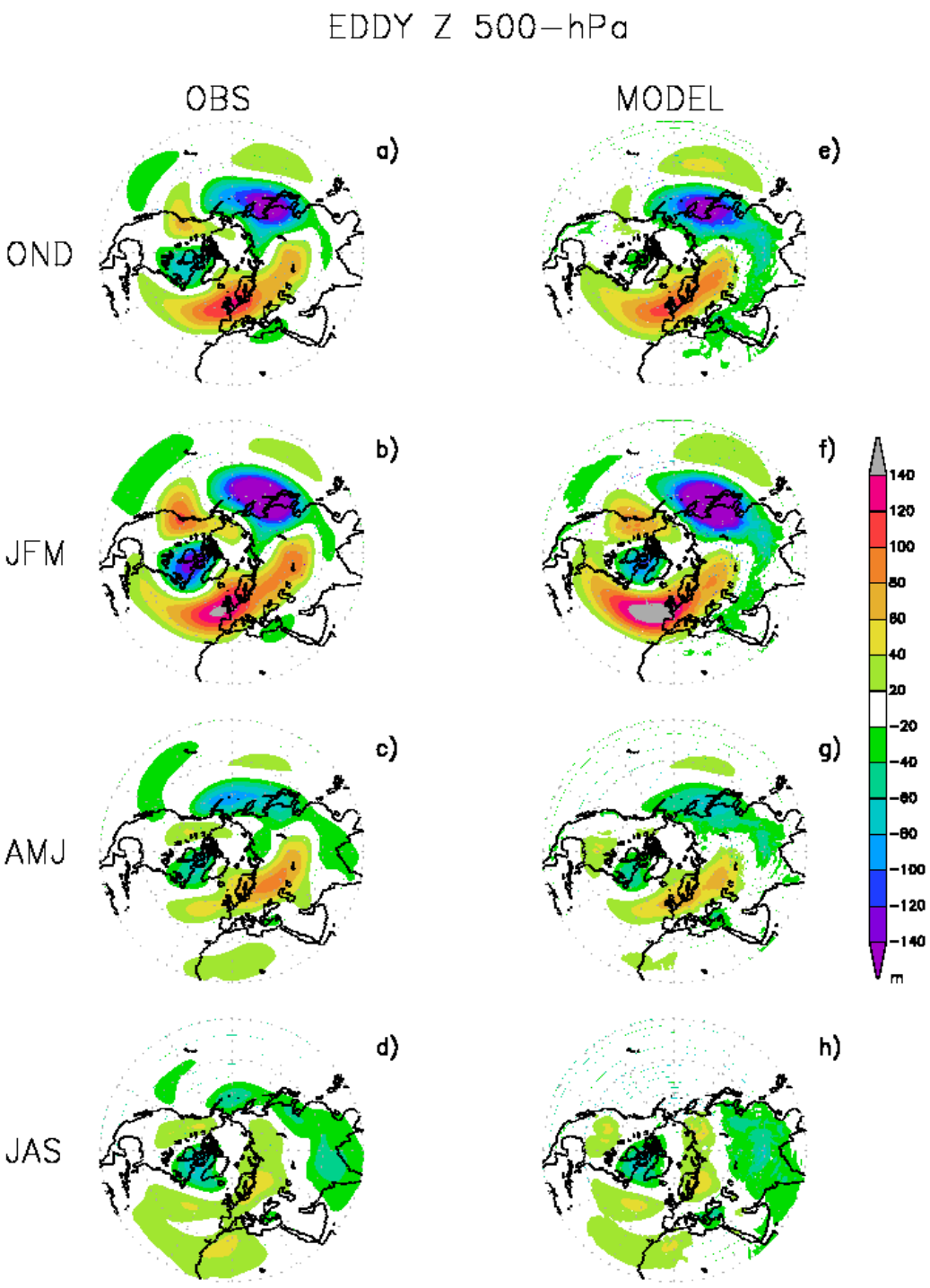

Fig. 3.5: as in Figure 3.3 but for seasonal means of eddy component of the geopotential height (Z) at 500 hPa. the eddy Z has been computed by subtracting the zonal mean to the total field. The shaded contour interval is 20 metres.

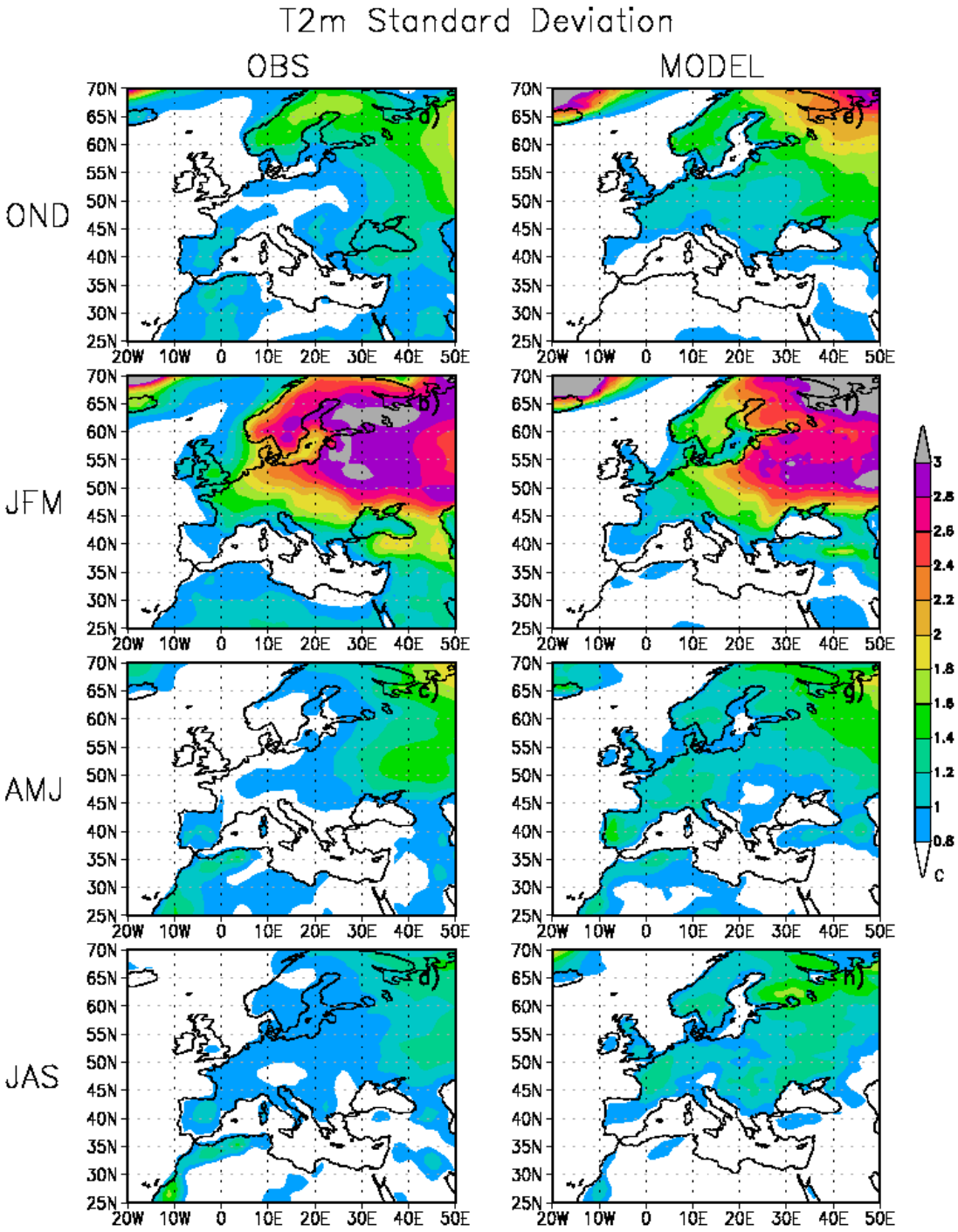

Fig. 3.6: Standard deviation of the seasonal values of T2m during the period 1961-1990 for the observations (left column) and model simulation (right column). Shaded contour is 0.2°C.

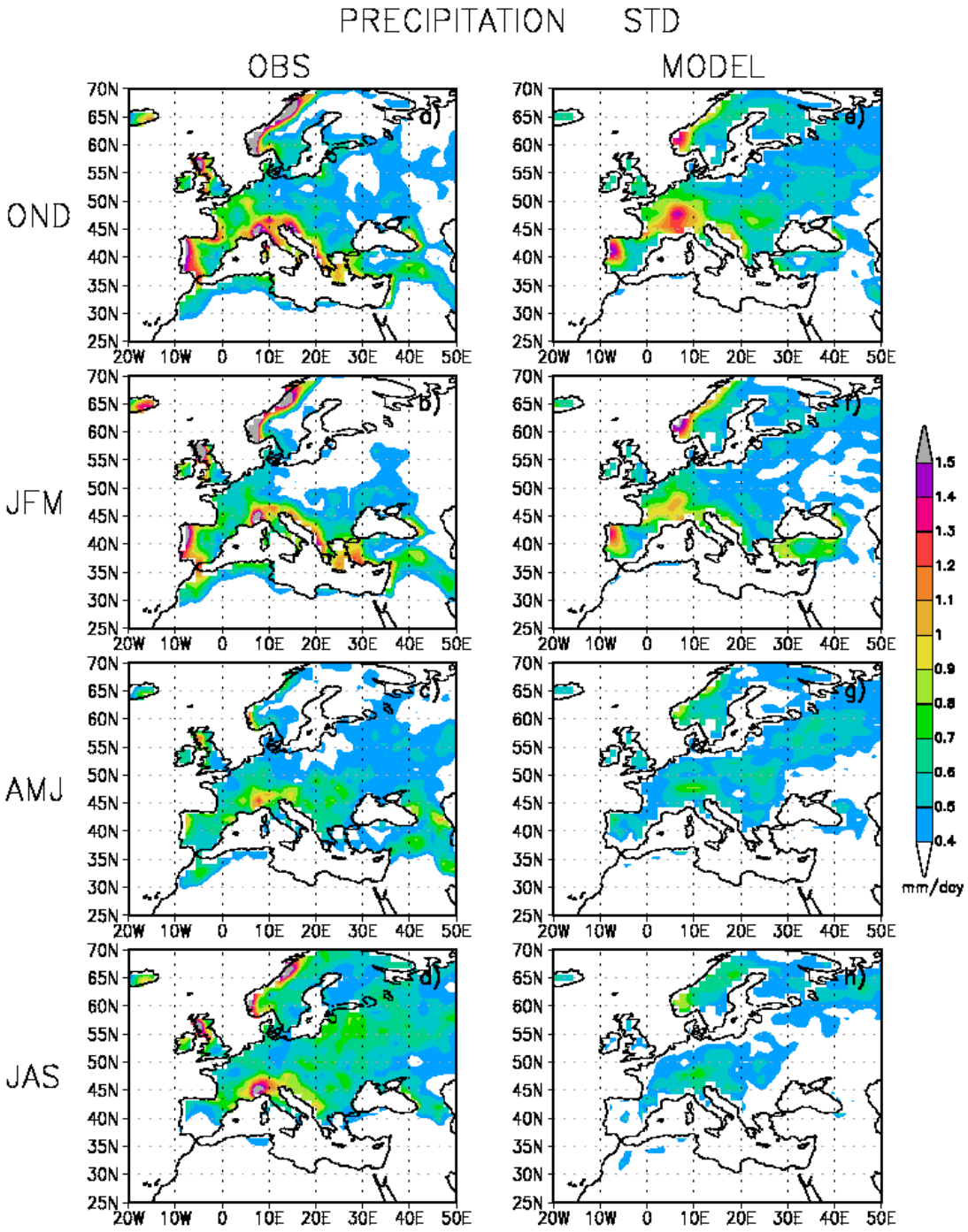

Fig. 3.7: as in figure 3.6 but for the observed and simulated precipitation. Shaded contour interval is 0.1 mm/day.

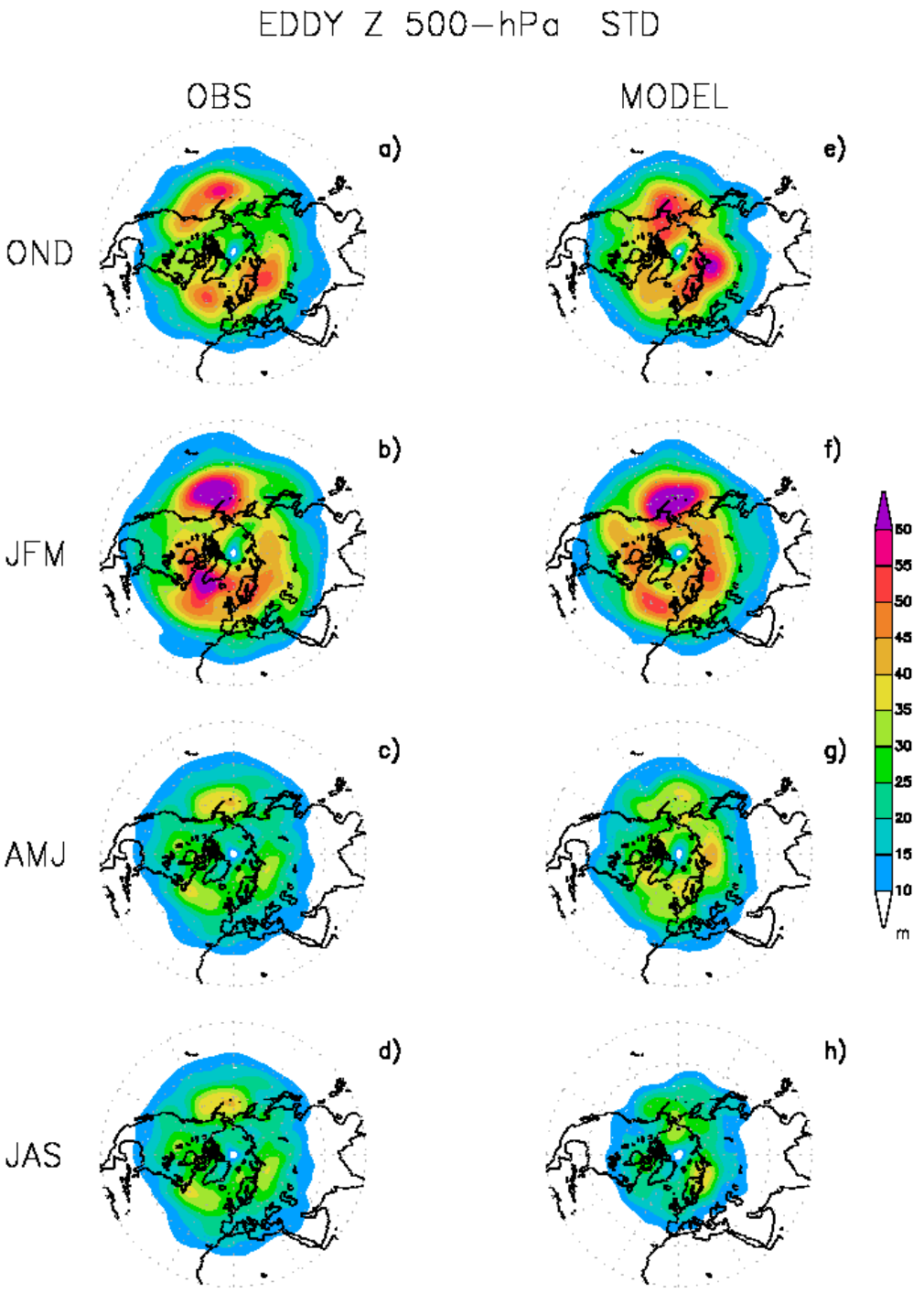

Fig. 3.8: Standard deviation of the seasonal values of the eddy component of the 500 hPa geopotential height (Z500). Left column observations. Right column 20C model simulation. Shaded contour interval is 5 m.

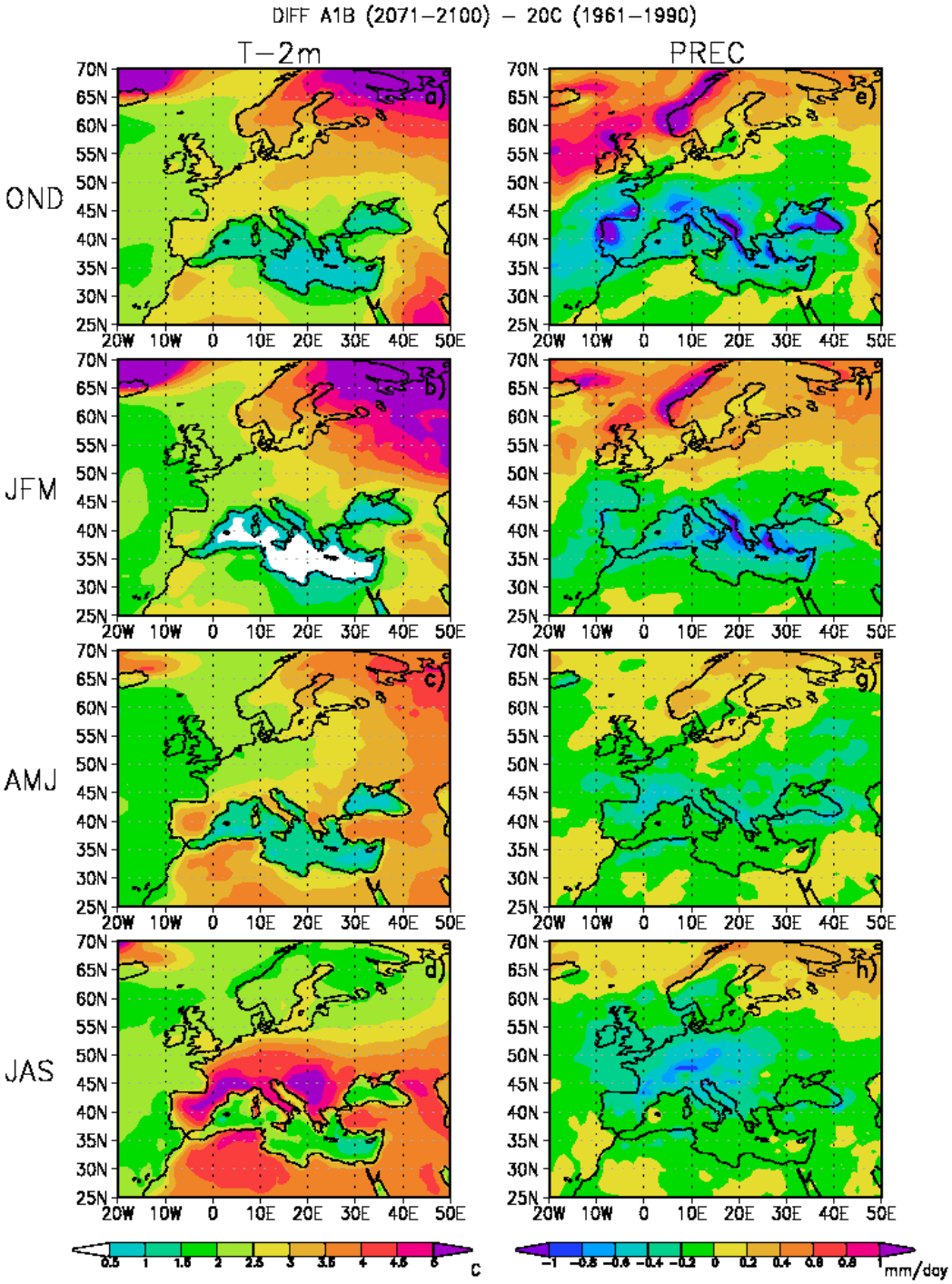

Fig. 3.9: Difference between the seasonal means of T2m (left panels) and precipitation (right panels) seasonal mean during the simulate 1961-1990 period and the 2071-2100 A1B simulation. The shaded contour interval for precipitation is 0.5°C; the contour interval for the precipitation field is 0.2 mm/day.

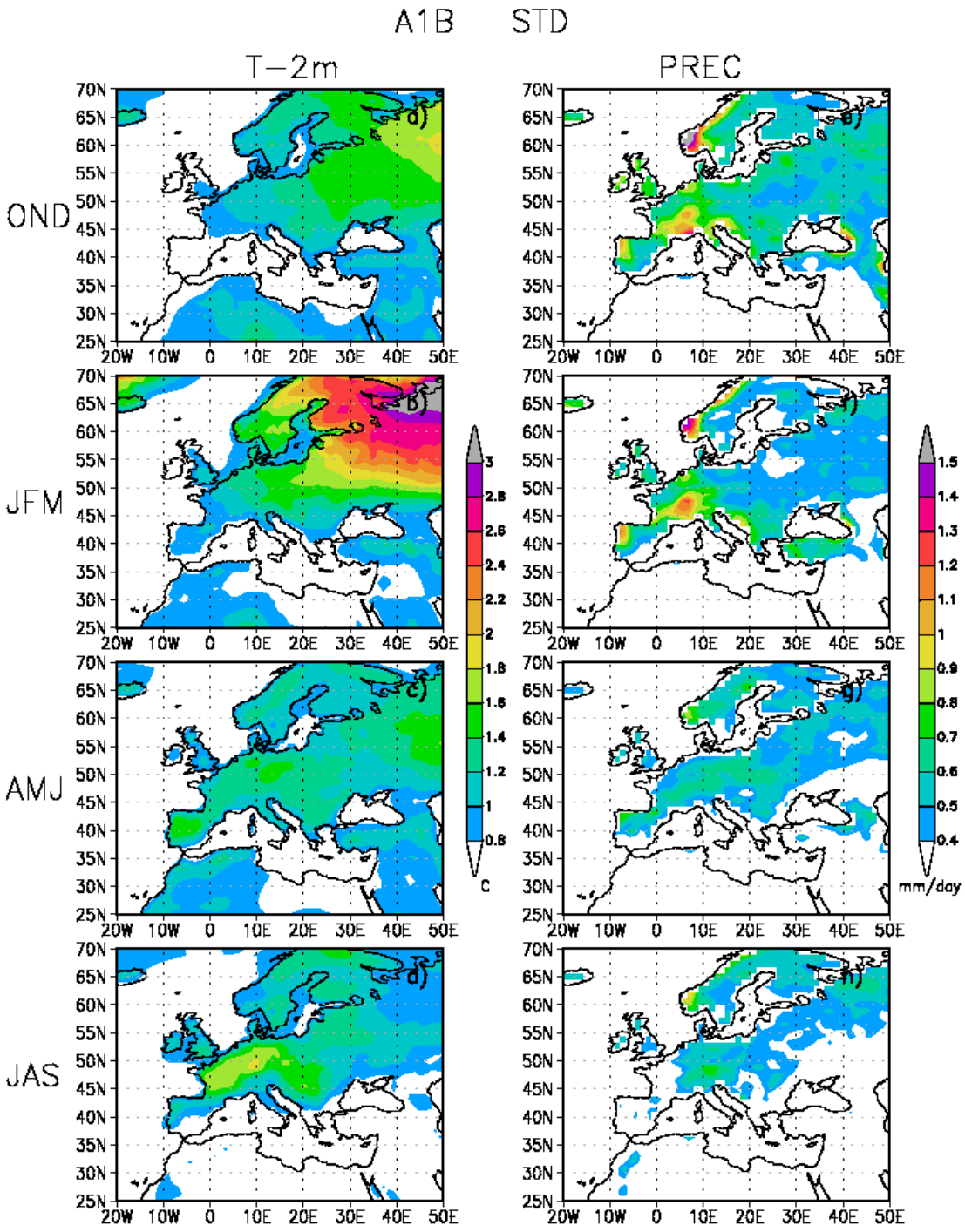

Fig. 3.10: Standard deviation of the seasonal values of T2m (left column) and precipitation from the A1B scenario simulations. The seasonal means have been computed for the period 2071-2100. Contour interval is 0.2°C for the T2m field and 0.1 mm/day for the rainfall standard deviation.

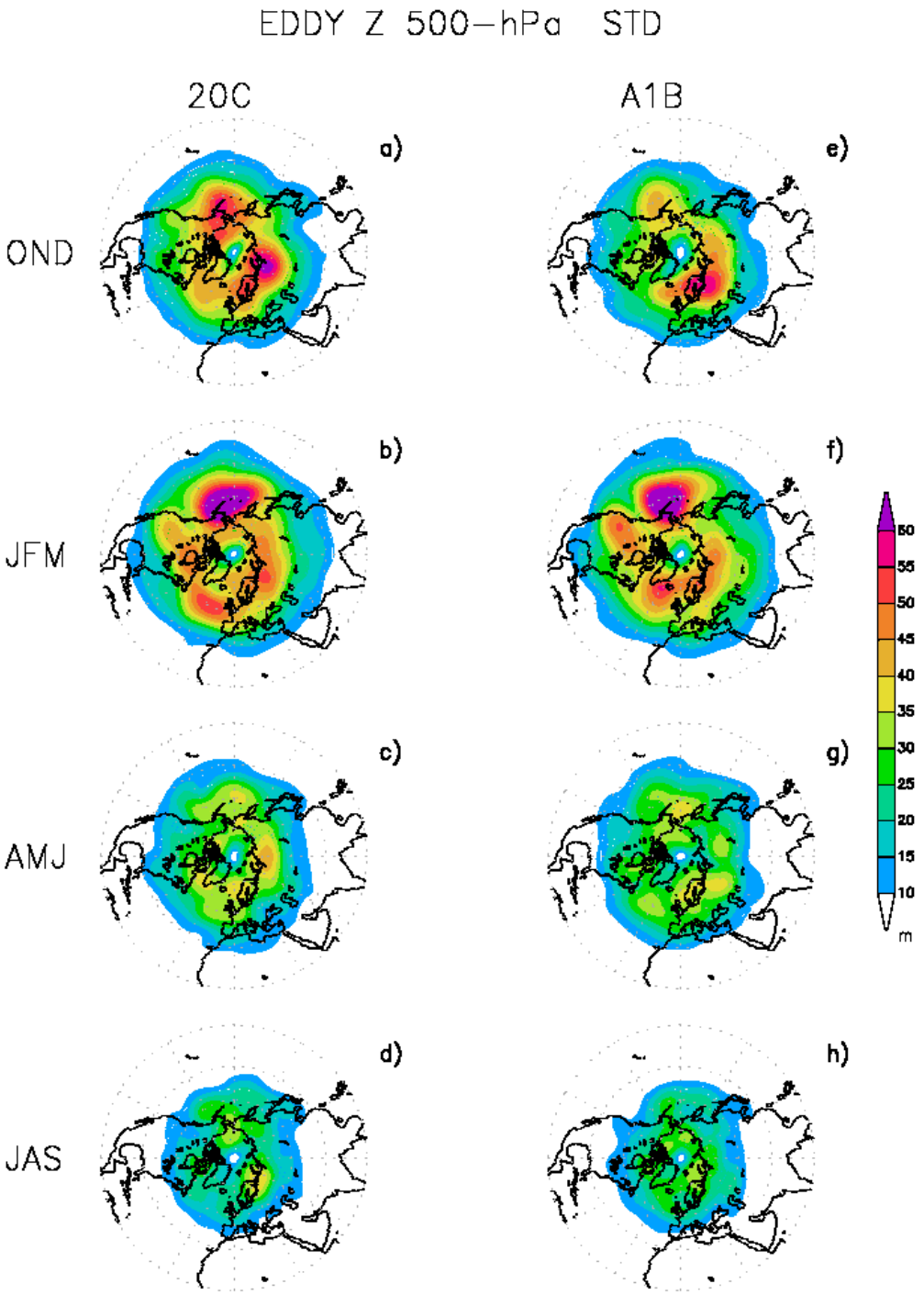

Fig. 3.11: Standard deviation of the seasonal values of the eddy Z500 obtained from the 20C model simulation (left panels) and the A1B scenario simulation (right panels). Contour interval is 5 m.

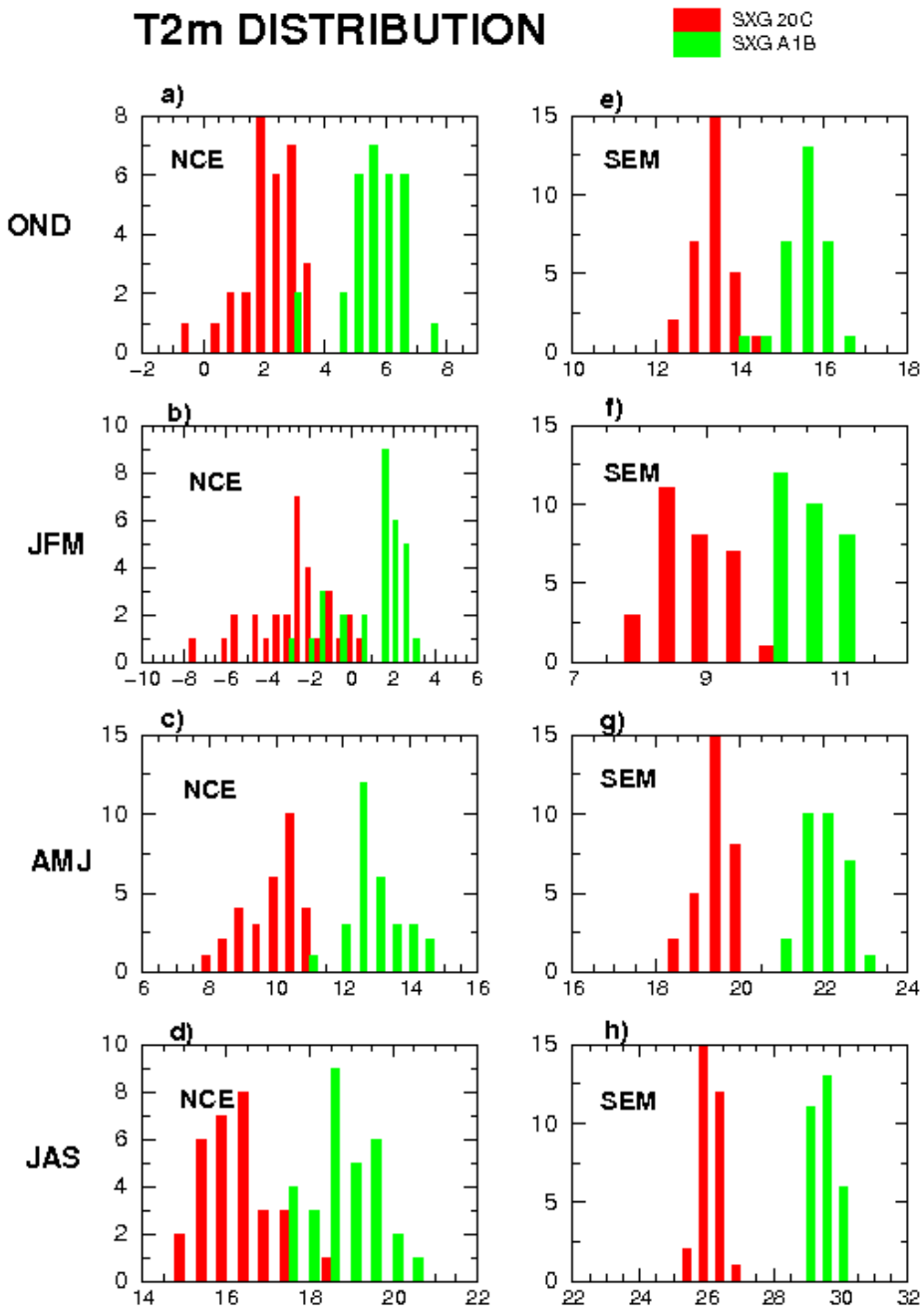

Fig. 3.12: Distributions of T2m as obtained from the 20C simulation seasonal means (red bars) for the period 1961-1990 and from the A1B scenario simulation (green bars) for the period 2071-2100. On the x-axes are the temperature values in °C (the temperature bin is 0.5°C); on the y-axes are the number of events.

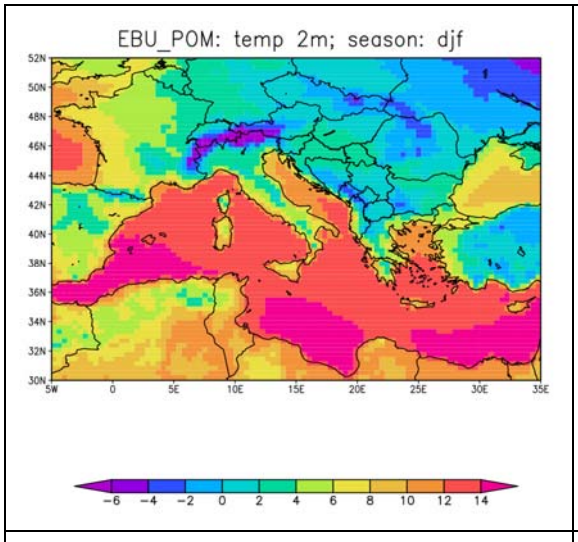

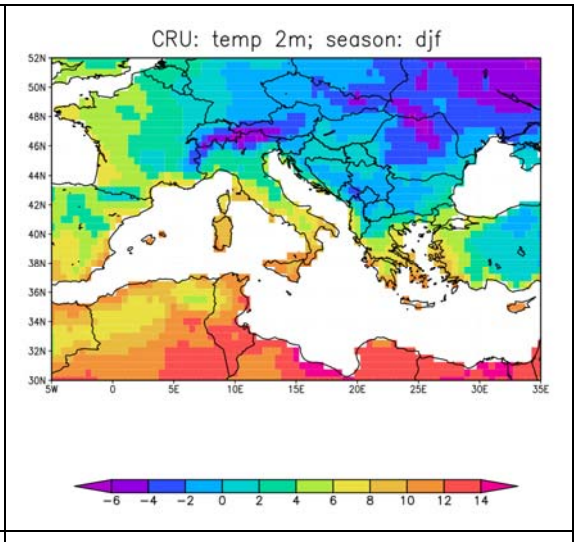

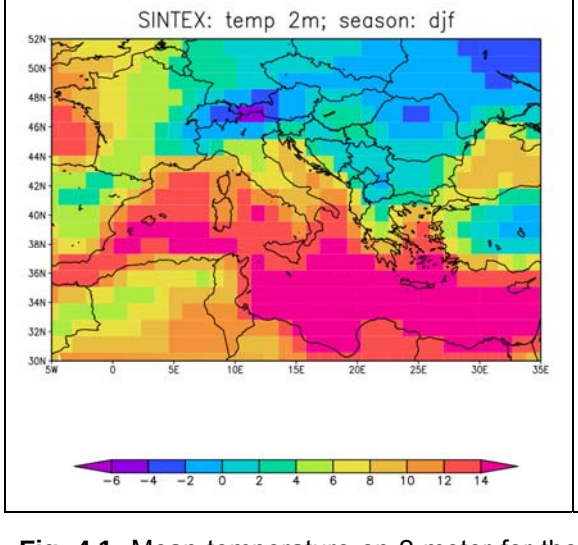

	BIAS	***MAE***	***RMSE***
CRU	-0.21	1.88	2.15
WM	-0.06	1.97	2.28

Fig. 4.1: Mean temperature on 2 meter for the DJF season, top left from CRCM, top right from the CRU data set, bottom left from SINTEXG and bottom right CRCM scores in the form of *bias, mae* and *rmse* calculated using two data set CRU and WM.

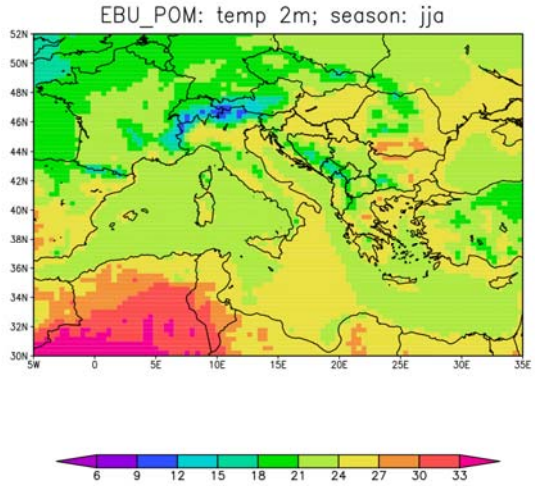

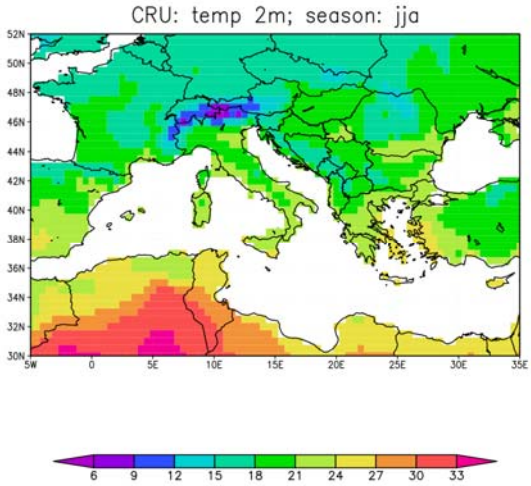

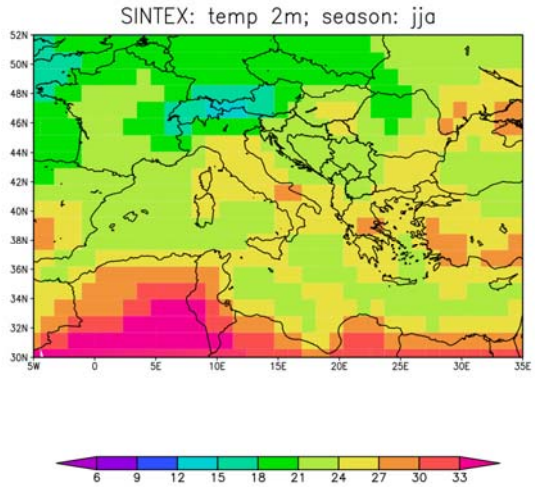

	BIAS	MAE	RMSE
CRU	2.63	2.96	3.42
WM	2.57	2.99	3.50

Fig. 4.2: The same as in Fig. 4.1, but for the JJA season.

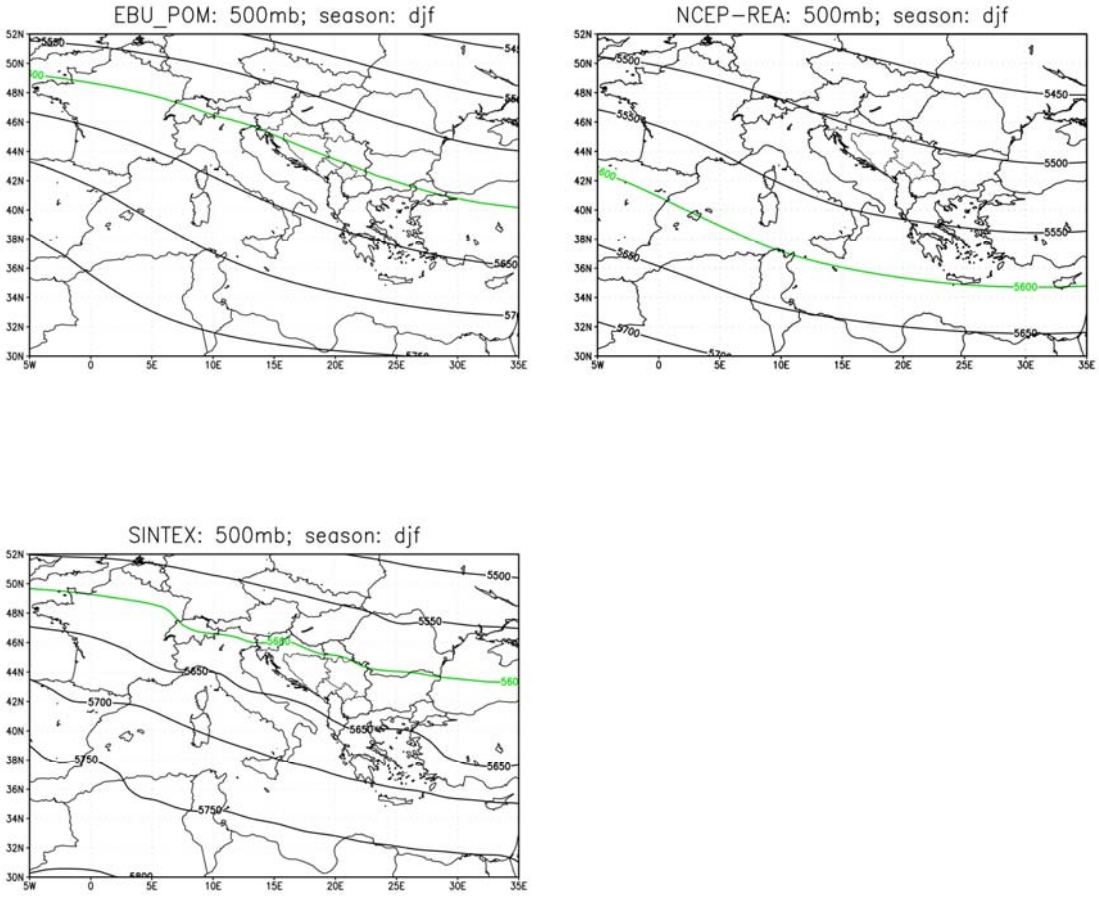

Fig. 4.3: 500 mb geopotential fields for the DJF season. Top left from CRCM, top right from the NCEP-reanalysis data set, bottom left the global filed.

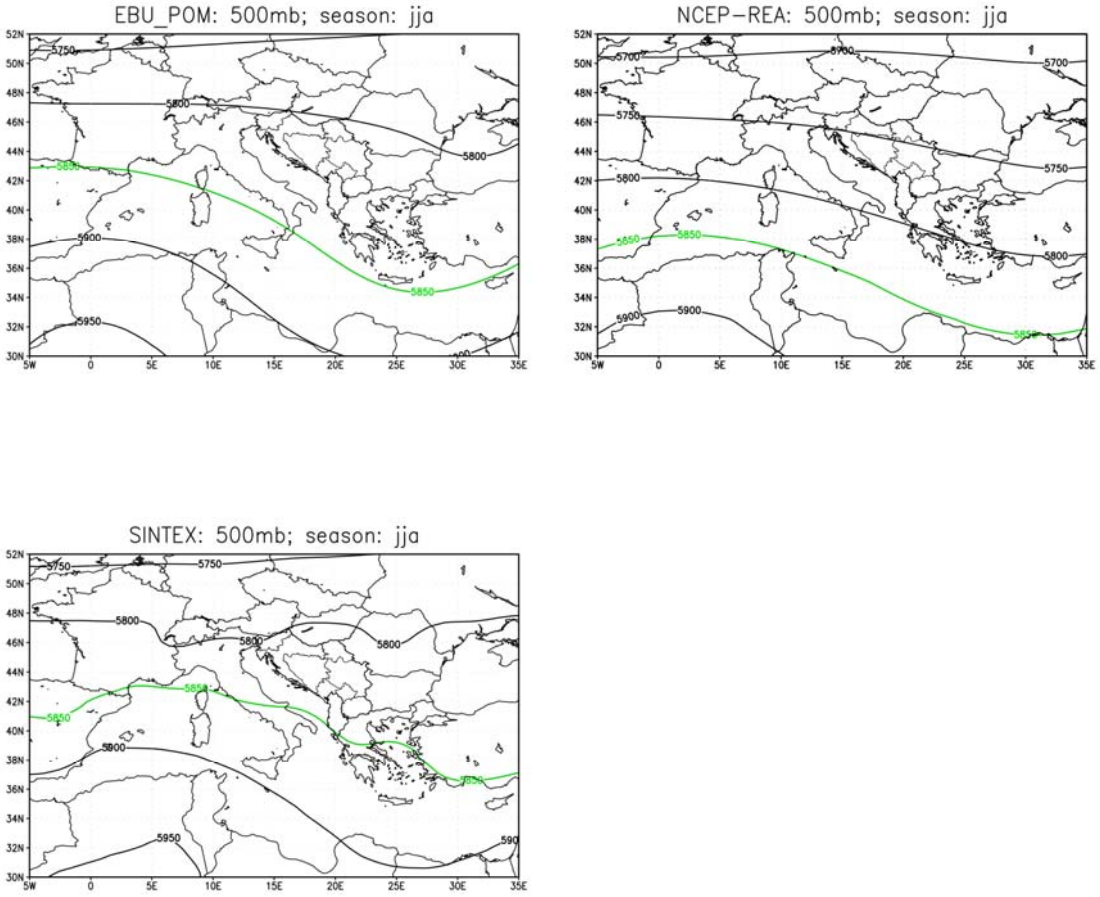

Fig 4.4: The same as in Fig. 4.3 but for the JJA season.

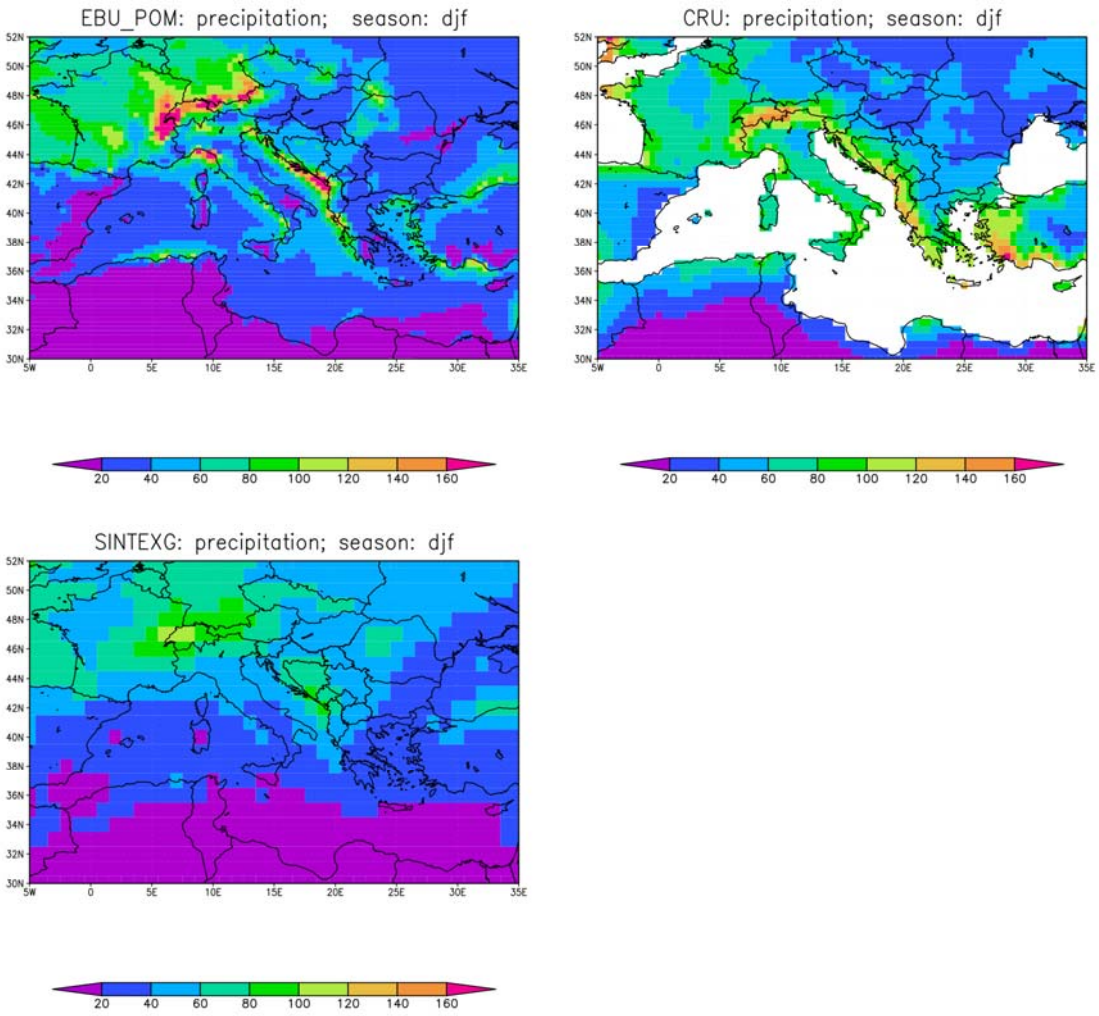

Fig. 4.5: Monthly accumulations of precipitations (mm/month) for the DJF season, top left from CRCM, top right the from the CRU data set, bottom left global.

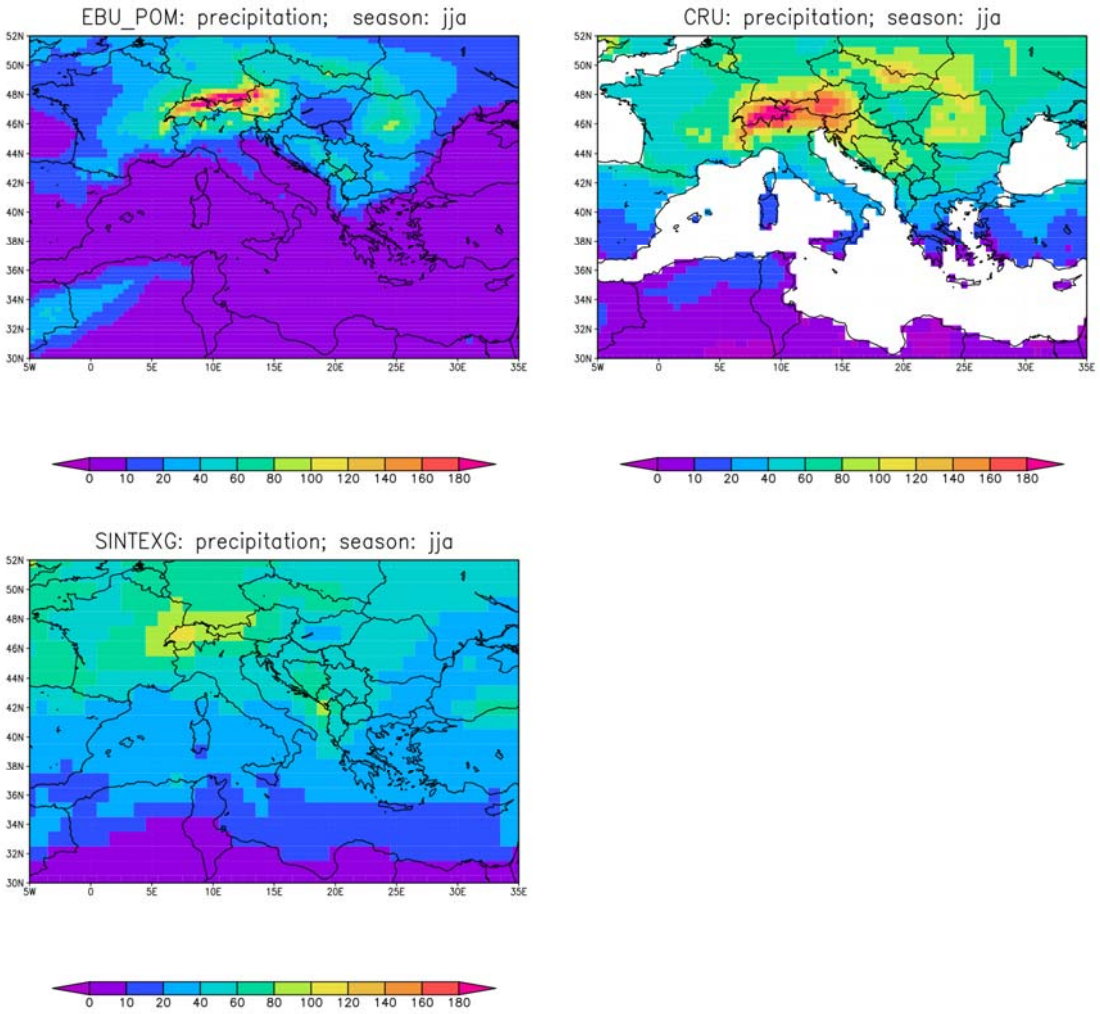

Fig 4.6: The same as in Fig. 4.5 but for the JJA season.

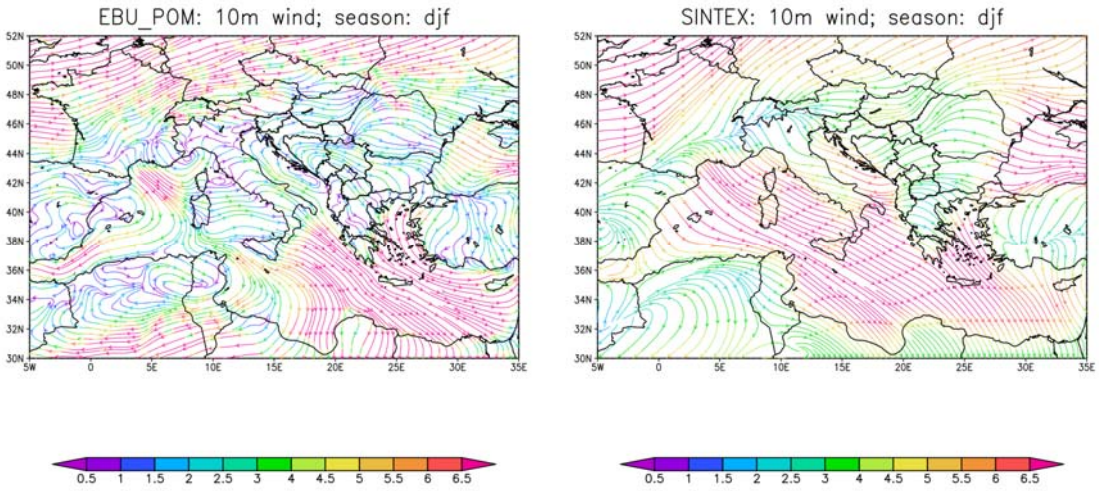

Fig 4.7: Present climate winds for the DJF season. On the left CRCM results and on the right SINTEXG results, with coloring from weak winds in purple to strongest wind in red.

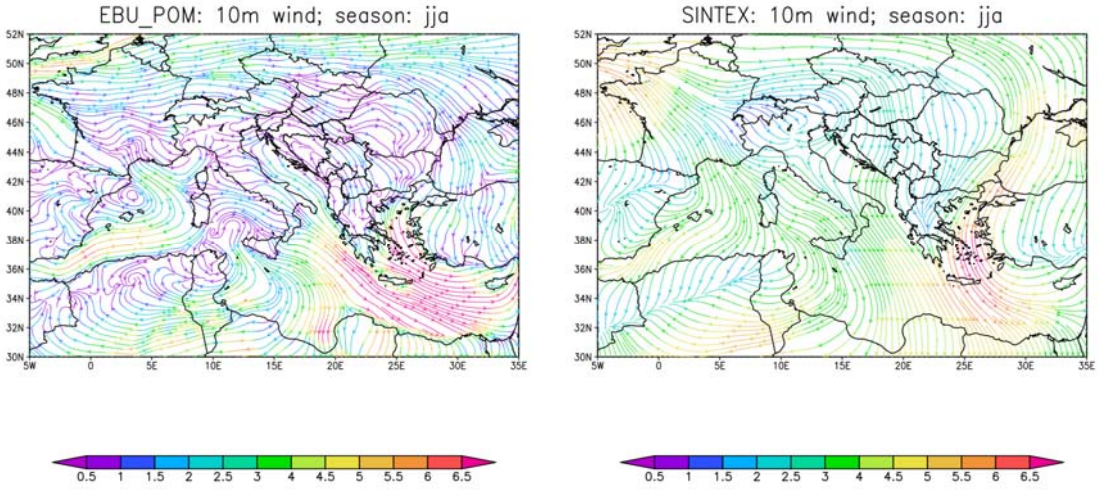

Fig. 4.8: The same as in Fig. 4.7, but for the JJA season.

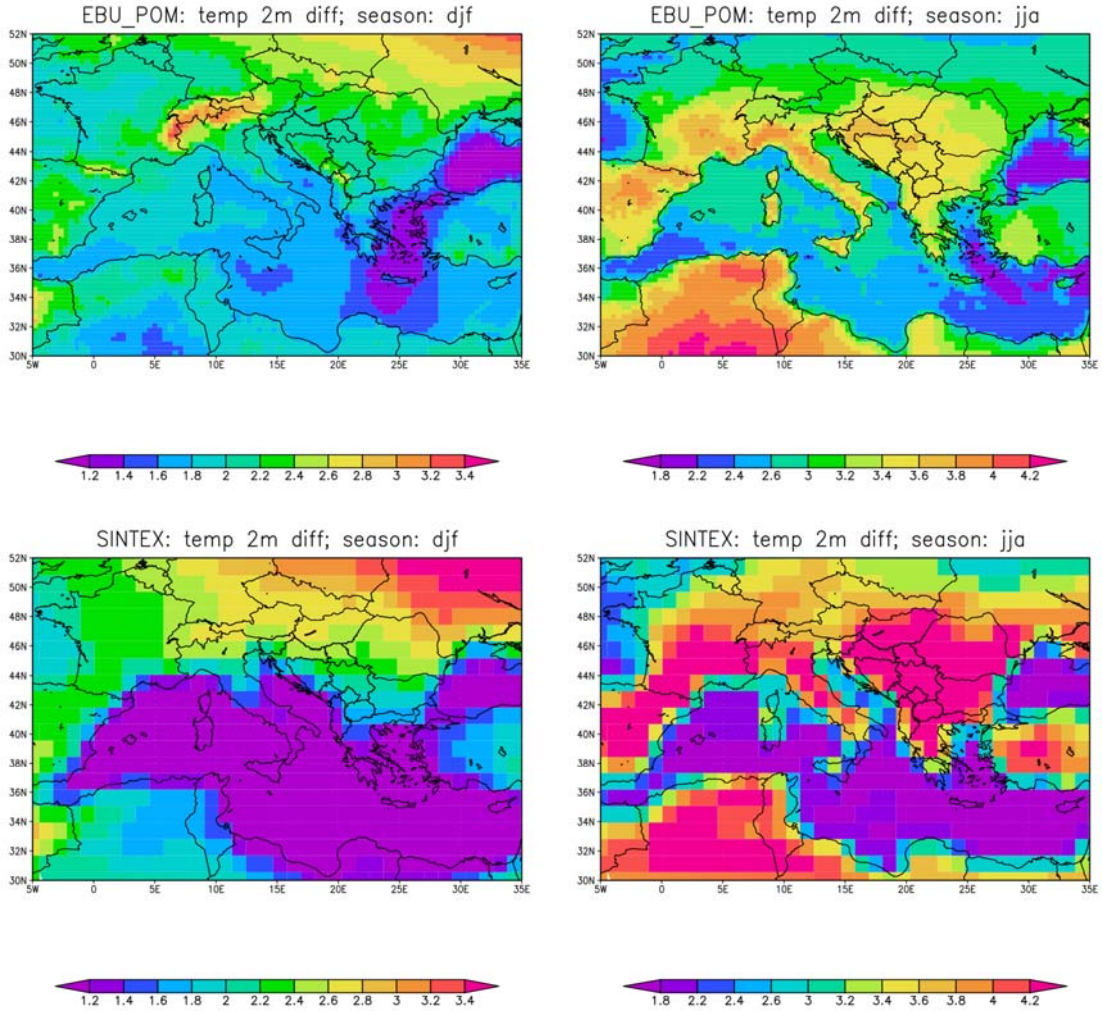

Fig. 4.9: Differences between future climate (21st cen.) and present climate (20th cen.) for T2m field. Top right the CRCM simulations for the DJF season, top left the CRCM simulations for the JJA season. Bottom panel the same but for the global simulations.

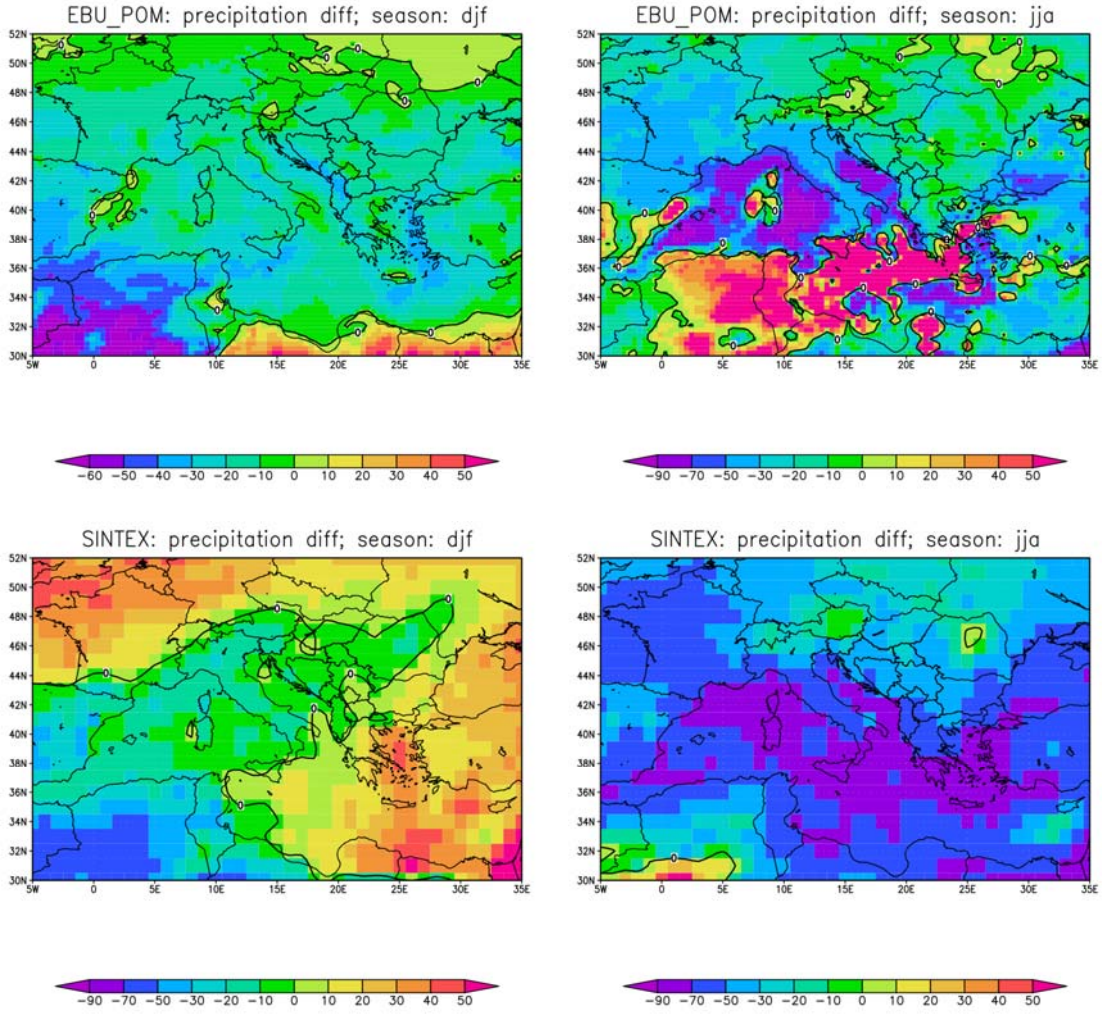

Fig. 4.10: The same as in Fig. 4.9, but for the precipitation.

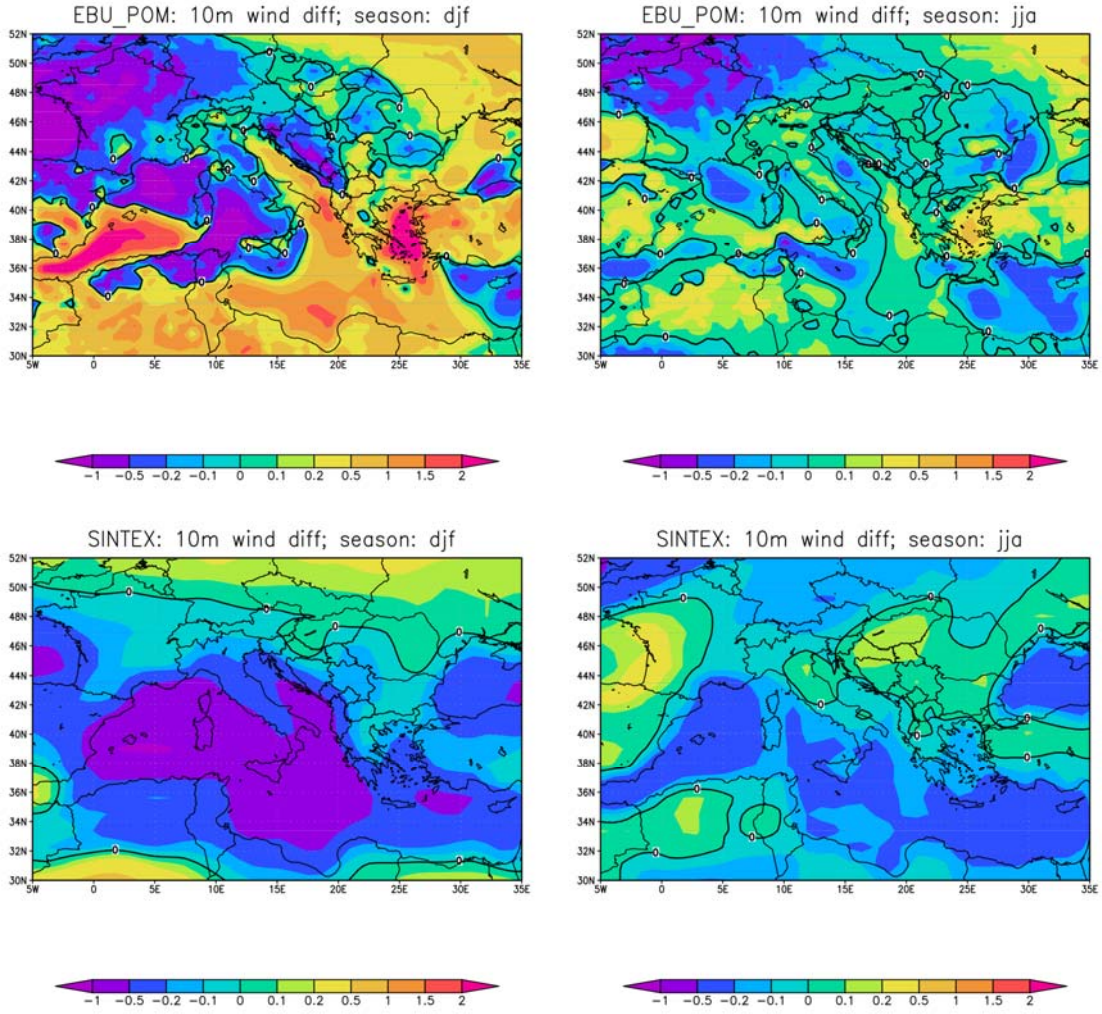

Fig. 4.11: The same as in Fig 4.9, but for 10m wind, its intensity.

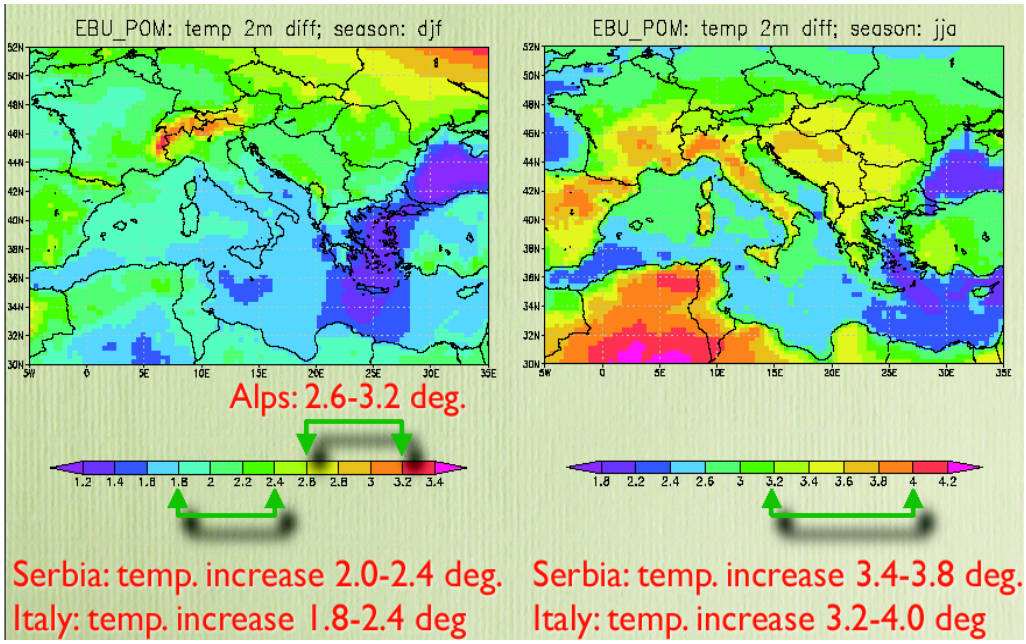

Fig. 5.1: Regional simulations of T2m from the CRCM for DJF season, on the left, and JJA season on the right.

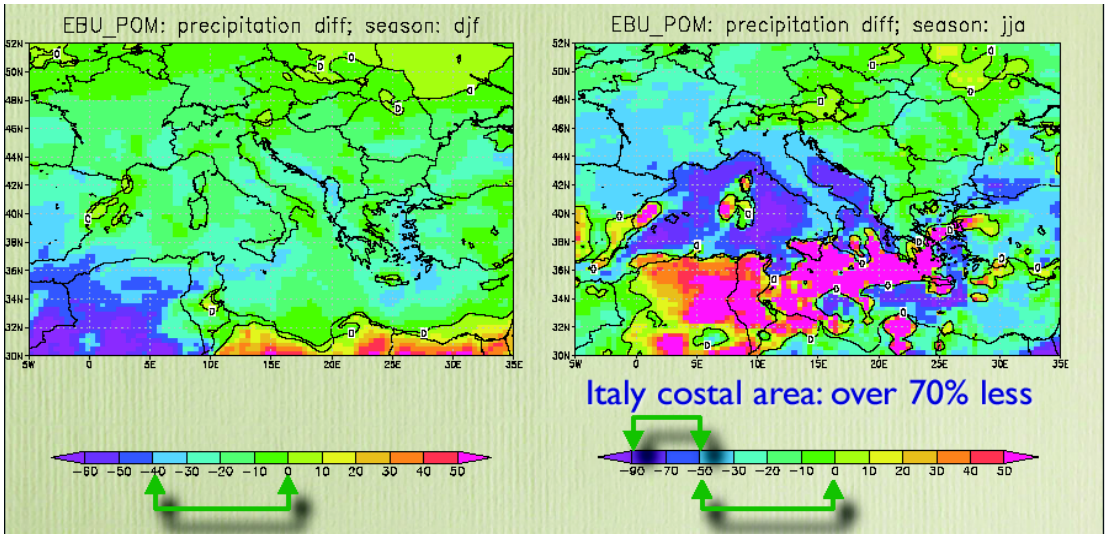

Fig. 5.2: Regional simulations of precipitation from the CRCM for DJF season, on the left, and JJA season on the right.

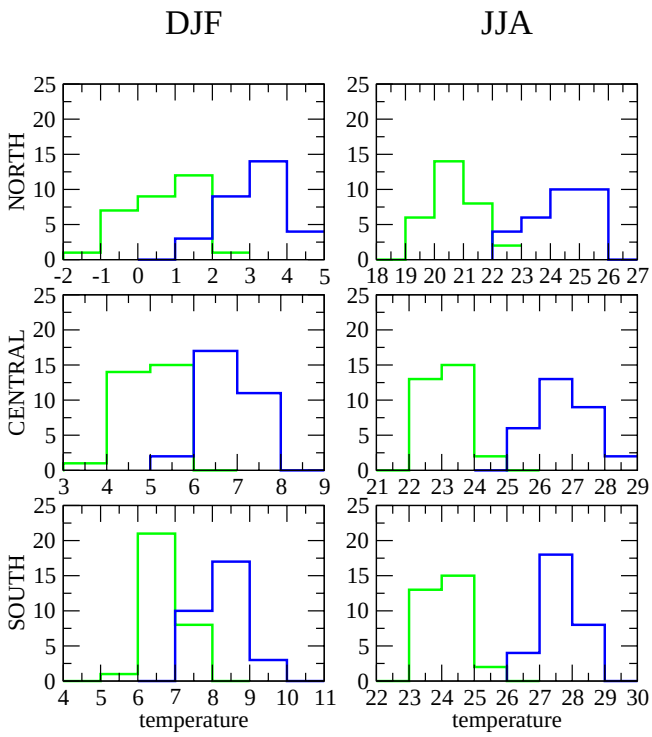

Fig 5.3a: Regional distributions of temperature for different parts of Italy. Numbers on the ordinate axis represent number of years with temperature bin on the horizontal axes, out of whole time slice of 30 years. The green line is for the present climate and the blue is for the future climate.

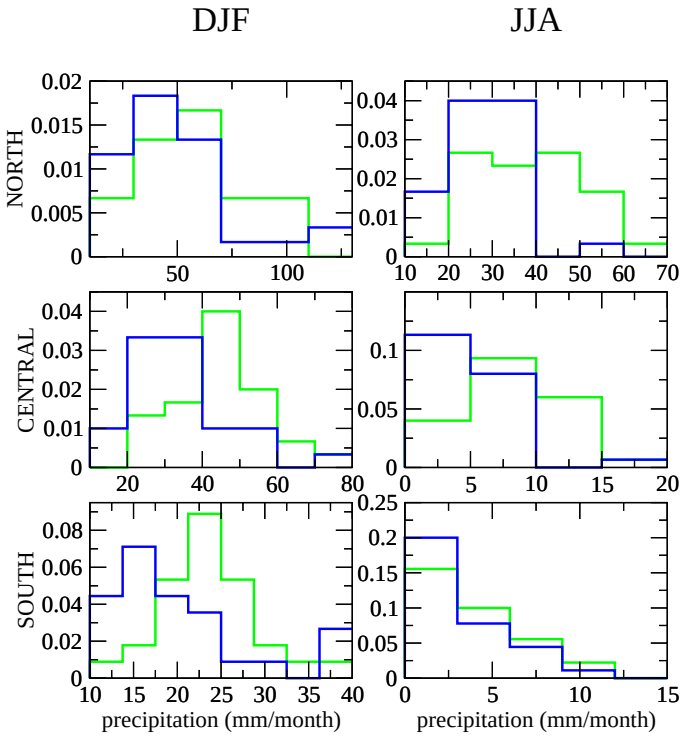

Fig. 5.3b: The same as in Fig. 5.3a but for the precipitation.

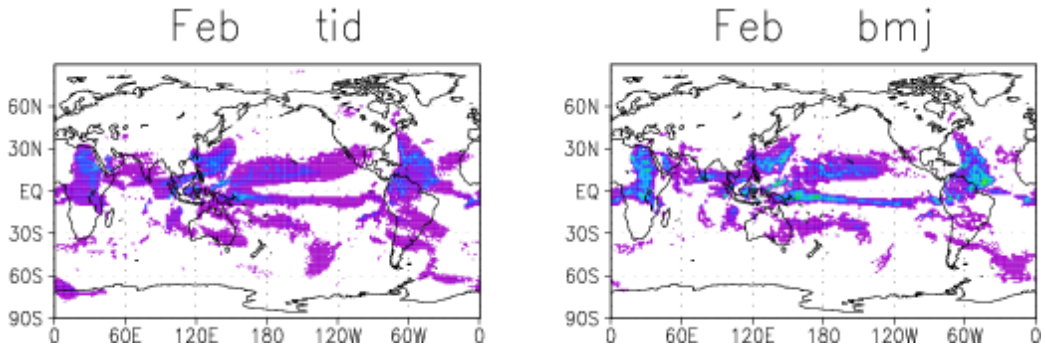

Fig. 6.1a: Latitude-longitude distribution of cumulus heating rates shown in the form of accumulated precipitation for the second month of integration (in mm/month). The left row of panels has the Tid cumulus scheme while the right row of panels has the BMJ cumulus scheme.

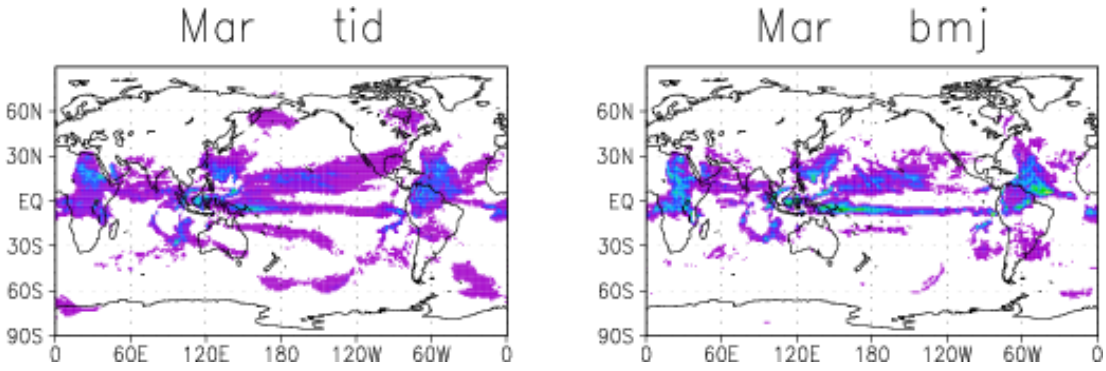

Fig. 6.1b: The same as in Fig. 6.1a but for the second month of integration.

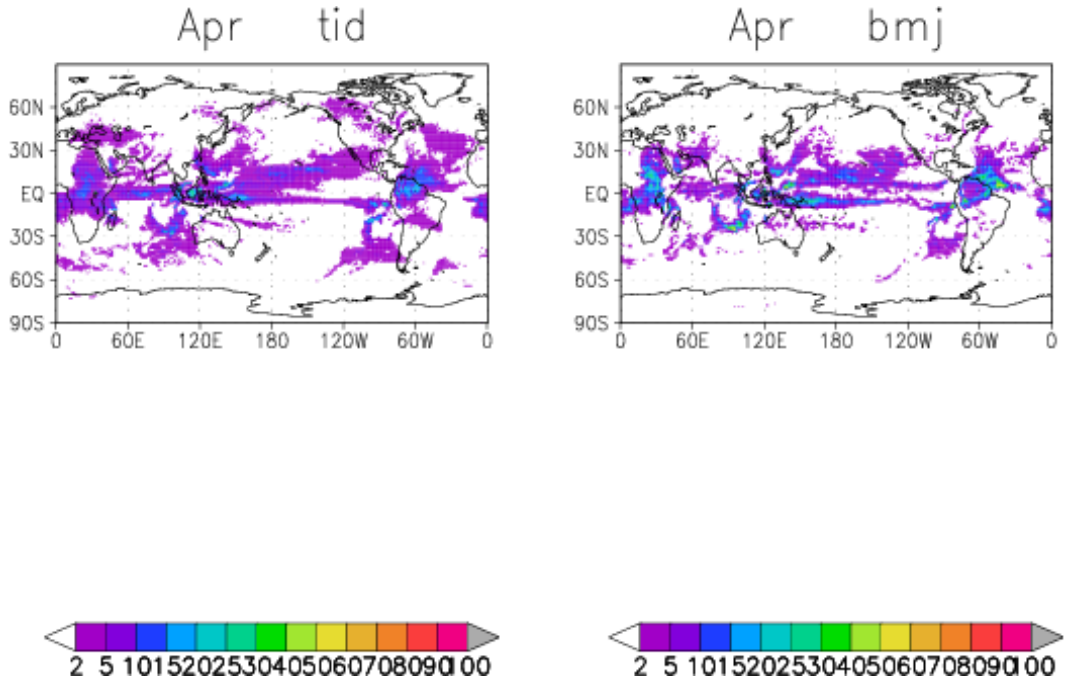

Fig. 6.1c: The same as in Fig. 6.1a but for the third month of integration.

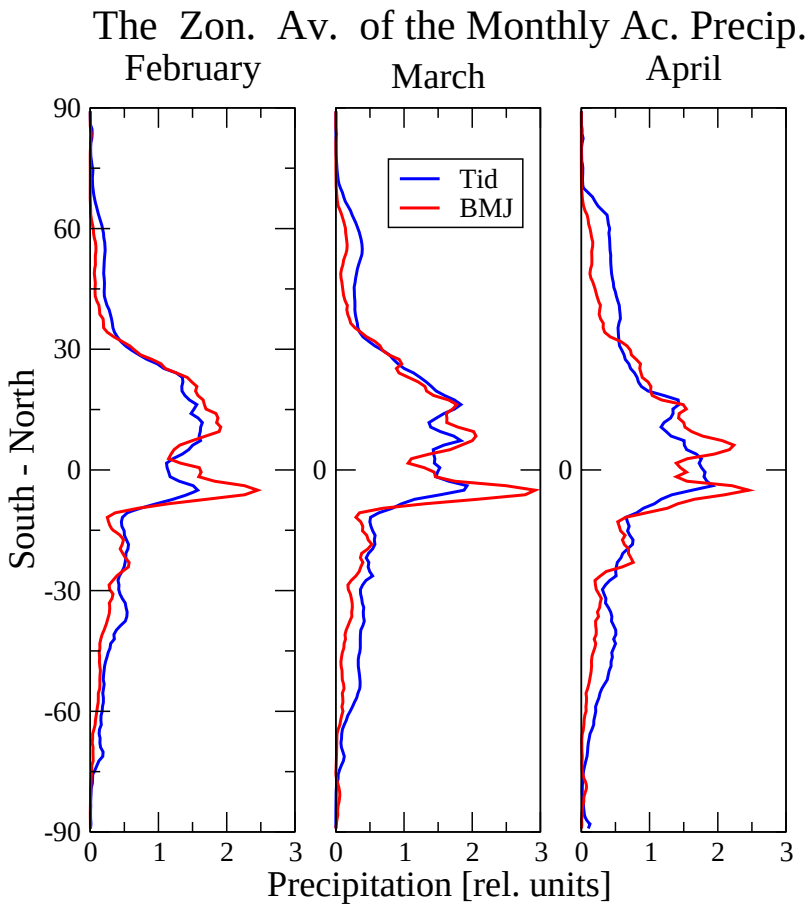

Fig. 6.2: Zonal averages of the monthly mean precipitation. Blue represents profiles obtained by the Tid scheme while red profiles are from the BMJ scheme.

ANNEX 1: THE BETTS-MILLER-JANJIC CONVECTION SCHEME

Deep convection

The BM and BMJ schemes belong to the wider class of the so called adjustment scheme. The first such scheme was the moist adjustment scheme (Manabe et al 1965, Kurihara 1973). In that same group belongs Kuo (1965, 74) scheme. Actually BM, BMJ and Kuo shame are of the same form. All force vertical profiles of temperature and moisture towards some value i.e. they are lagged convective adjustment over time but with different time scale. Beside that the profiles towards which the adjustment is done are also different. In this manner all schemes avoid the biggest weakness of the Manabe's scheme, sudden changes in profiles and therefore sudden changes in forcing producing strong numerical noise. The calculation of deep convection heating starts with specification of the *cloud bottom*. Starting from the several lowest levels a parcel is lifted to its lifting condensation level (LCL) and its equivalent potential temperature Θ_e is calculated there. The starting level from which the parcel has the highest Θ_e is the bottom of the cloud. Hat has been schematically presented in **Fig. A1.1**.

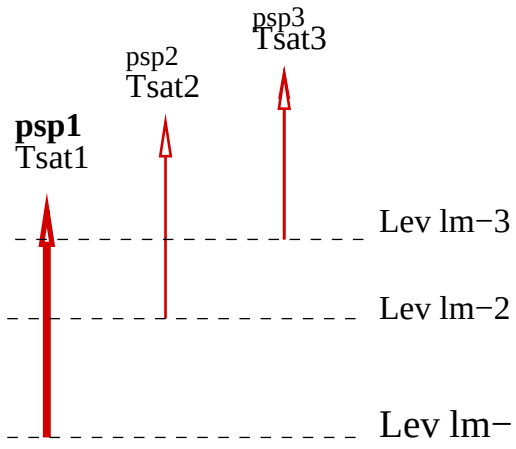

Fig. A1.1: Schematic presentation of the search for the clod bottom through lifting parcels for several lowest levels to their LCL. Parcel with the highest equivalent potential temperature determines the level at which the clod bottom is (darker red in this example).

Once we have determined the cloud bottom we precede with the calculation of the *preliminary* reference profiles for temperature and humidity. The first part of the temperature reference profile, from the cloud bottom to the *freezing level*, is obtained integrating the equation:

$$\frac{\partial \theta^{1}_{ref}}{\partial p} = S_{deep} \frac{\partial \theta_e}{\partial p}$$

Here S_{deep} is a constant, close but smaller then one, determining the stability of the profile. The second step is search for the *cloud top*. It is placed at the highest level where T_{mad}, temperature of the moist adiabat, exceeds the temperature of the column that we are considering. Here the scheme has the first of several pre-imposed limits. In order to be considered as a deep cloud its distance between the cloud top and bottom should be larger then some prescribed minimum (currently 290 mb).With defined values of the reference profile, at the freezing level and cloud top,

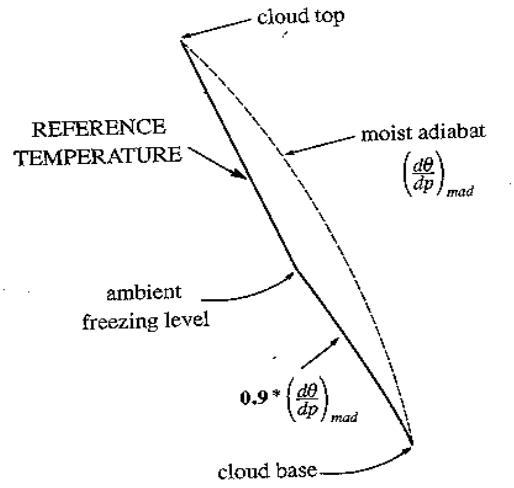

Fig. A1.2: Construction of the first guesses temperature reference profile for deep convection. Starting with the cloud bottom the equivalent potential temperature, slightly reduced, is integrated upwards to the freezing point. From there linear interpolation in pressure to the previously determined cloud top.

we calculate it's values in between by linear interpolation over pressure. See **Fig. A1.2** for the schematic presentation of the process.

The humidity reference profile is expressed using the quantity: deficit from saturation pressure *dsp* in the following text, defined by Betts as:

$$dsp = p_{sat} - p \ ,$$

where *p* is pressure at a given level and p_{sat} pressure saturation level reached through dry adiabatic ascent starting from that level until the condensation starts. The idea is that scattering of the characteristic values for *dsp* is smaller then the corresponding actual humidity values. According to Betts, based on the numerous observations, all humidity reference profiles can be expressed by three characteristic numbers, presented in the **Table A1.1**, and then again the rest of the profile is obtained by linear interpolation in pressure.

Characteristic cloud level	notation	value of *dsp* in mb's
Top	dsp_{top}	-20
Freezing	$dsp_{freezing}$	-40
Bottom	dsp_{bottom}	-25

Table A1.1: Values (mb) of the *dsp* for three characteristic levels, top, freezing level and bottom of a deep cloud

As we mentioned these are only preliminary profiles. The final profiles are obtained by imposing the condition that enthalpy of the profiles is equal with enthalpy of the observed profiles or in the model with the profiles at the considered column. Actually we demand that integrals which mean that vertical mean values are the same:

$$\overline{H_{ref}} = \int_{top}^{bot} \left[c_p T_{ref}(p) + L_v q_{ref}(p) \right] dp = \int_{top}^{bot} \left[c_p T(p) + L_v q(p) \right] dp$$

Fulfilment of this condition is usually done through several iterations. First we find $\Delta\overline{H}$ difference between two integrals. If there is a difference we change the preliminary profiles. Since $H = H(T_{ref}, q_{ref})$ we can write:

$$\frac{\partial H_{ref}}{\partial T_{ref}} = c_p + L_v \frac{\partial q_{ref}}{\partial T_{ref}}$$

From which we get correction of T_{ref}^1

$$\Delta T_{cor} = \frac{\Delta H}{\frac{\partial H^1}{\partial T_{ref}^1}}.$$

The new humidity profile is then calculated using corrected temperature. Once referent profiles are formed we can get convective forcing:

$$T^{n+1} = T^n + \Delta t \frac{T_{ref} - T^n}{\tau}$$

$$Q^{n+1} = Q^n + \Delta t \frac{Q_{ref} - Q^n}{\tau}$$

where *n* is time level, *Δt* is the length of the time step and τ is fixed time relaxation coefficient. In **Fig A1.3** there is another illustration of the above process of calculating reference profiles, the first guess and the final ones.

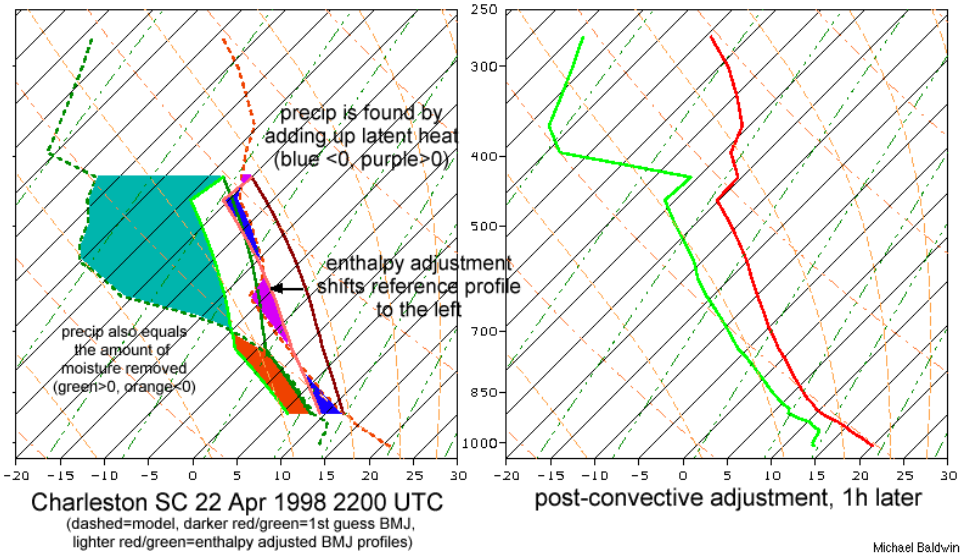

Fig. A1.3: Profiles of temperature and humidity as in the first guess and after adjustment after the enforcement of the enthalpy conservation (left) and resulting profiles 1 hour later (right). [From Michel Baldwin, 1996].

Amount of precipitation is diagnosed from the warming or from the moistening tendencies. Due to the imposed explicit conservation of enthalpy both numbers are the same:

$$Prec = \frac{\rho_w \Delta t c_p}{g \tau L_v} \sum_{bot}^{top} (T_{ref} - T)\Delta p = \frac{\rho_w \Delta t}{g \tau} \sum_{bot}^{top} (Q_{ref} - Q)\Delta p$$

In the case that diagnosed amount of precipitation is negative, deep convection is abandoned and changed to shallow convection, with new height of the cloud top, in Betts term *switch* is made.

Shallow convection

Although the shallow convection scheme at this moment has not been implemented in the SINEXG model for the completeness we will include its description in the report. Perhaps the deep convection basic ideas are better understandable when the other is present. The role of the shallow convection is to prepare pre-convective environment via vertical mixing by transporting moisture upward and temperature downward. It mimics process of condensation near cloud base as warming and drying and evaporation near cloud top through cooling and moistening without producing precipitation. As the shallow convection is diagnosed as the "swap" from the deep convection either because cloud top was too low or if the diagnosed rain was negative cloud bottom stays the same. The reference temperature profile is now calculated from the empirical fact that that shallow clouds are well mixed.

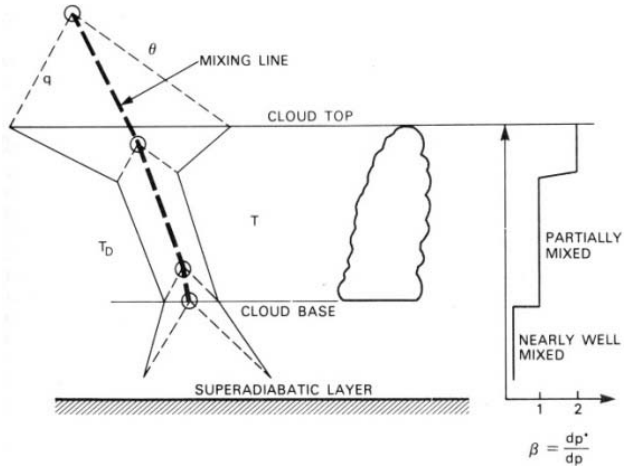

Fig. A1.4: Schematic representation of the shallow cloud, assuming that it is partially mixed through the cloud and well mixed bellow the cloud. Bottom and top of the cloud with profiles of potential temperature and specific humidity (From Stull, 1988)

In the case of the shallow convection dsp_{top} is drier then the one for the deep convection and the top of the cloud is moved one layer up. From the hypothesis that state is close to well mixed we get reference temperature profile from:

$$\frac{\partial \theta^{1}_{ref}}{\partial p} = S_{shall} \frac{\theta_{bot} - \theta_{top}}{p_{sat\_bot} - p_{sat\_top}}$$

Starting one level bellow the cloud up to the new, raised, top of the cloud ,where $p_{sat\_bot/top}$ are saturation pressures at the bottom and top of the cloud respectively. At the newly defined cloud top preliminary temperature and dsp_{top} are increased to strengthen always present inversion at the top of shallow clouds. This is graphically shown in the **Figs. A1.4** and **A1.5**. The condition of conservation of enthalpy, which operationally means its vertical mean, is also present in the calculation of the reference profiles for the shallow convection. Due to the fact that now we do not have precipitation, conservation of enthalpy is enforced separately for temperature and separately for specific humidity. In the end convective forcing is governed by the same relations as in the case of the deep convection.

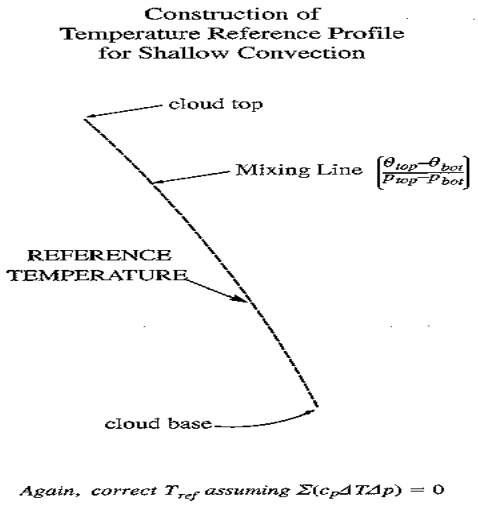

Fig. A1.5: Schematics of the reference profile for the shallow convection case and its relation to the clod base, top and assumption that profile is well mixed resulting in the queasy constant temperature gradient thought the cloud.

Modification of the BM scheme

The original BM scheme has been implemented by Z. Janjić into NCEP model and it was quite successful in generating and maintaining circulations whose source was convection. Comparison was made with some of the schemes of the Kuo type. Even tropical cyclone forecasts were successful in several cases (Lazić 1993, Janjić 1994). Further tests judging by the objective scores as well as by subjective inspection made it superior to some of competition schemes, in forecasting convective precipitation especially if it the case of strong precipitation. But as the time went by from forecast to forecast problems emerged. They could be grouped into three categories:

- perpetual rain over "warm" waters,

- weak precipitation over large areas over the ocean,
- entropy changes become very small resulting in pseudo-adiabatic profile

In order to reduce these problems Janjić introduces several modifications in both deep and shallow convection parameterization.

Modified deep convection

After extensive testing and experimenting Janjić traced the problem of the occasional excessive rains to the value of the time relaxation constant τ. He concentrated on the entropy profile and its evolution during these erroneous episodes of excessive rains. To quantize the processes he introduced a diagnostic variable the "entropy change" as:

$$\Delta S = \sum_{top}^{bot} \frac{c_p \delta T + L_v \delta q}{T} \Delta p$$

The reason why this parameter was particularly "suspicious" was that its value was *reduced* by a large amount during the convective episode approaching zero while the precipitation per time step was *increasing*. The ration between the two was up to 50 times bigger at the end of a convective episode in comparison with the beginning of the episode. The second fact was that occasionally there were instances when positive amount of rain was accompanied by the negative change (decrease) in entropy. When this was diagnosed calculation was stopped by neglecting changes coming from such step. With this intervention situation did improve but not in all cases. Sensitivity tests revealed that: increase of τ, in some cases did reduce the excessive rain. But increase everywhere gave wrong precipitation in other places, where wrong convective precipitation was replaced by the wrong large scale precipitation. These tests also showed that the scheme was sensitive to stability of the reference profiles. None of these changes, or their combination, was able to stop completely the problem in all cases.

The problem of the excessive rains could also be attributed to the excessive fluxes of moisture from the boundary layer. Problem can be even attributed to the excessive fluxes of moisture from the sea surface. Further analysis of the several very sever cases indicated that none of these were the likely candidates but the convection scheme itself, the assumption that τ being constants during the convective episode. In the modified version of the convective scheme it becomes a function of the new parameter, the so called "cloud efficiency" parameter defined as:

$$E = const \cdot \frac{\overline{T} \Delta S}{c_p \sum \delta T \Delta p},$$

where $\overline{T}$ is mean temperature between the cloud top and cloud bottom. Using parameter *E* this relaxation time constant can be modified as:

$$\tau_1 = \frac{\tau}{F(E)}$$

Due to the lack of data or information it was assumed that it is monotonous function, increasing with the increase of *E*. The simplest case of linear dependence was assumed. So at the beginning, with larger values of *E* starting relaxation coefficient is smaller and *increases* as *E* decreases with time. Beside this Janjić introduces the idea that reference profiles, particularly humidity one are not the fixed during the convective episode. Again due to the lack of the relevant information the simplest linear time variation was assumed. So convection starts with the "fast" profiles and gradually moves toward "slow" profiles as the *E* evolves. The idea is depicted in the schematic presentation bellow, in the **Fig. A1.6**.

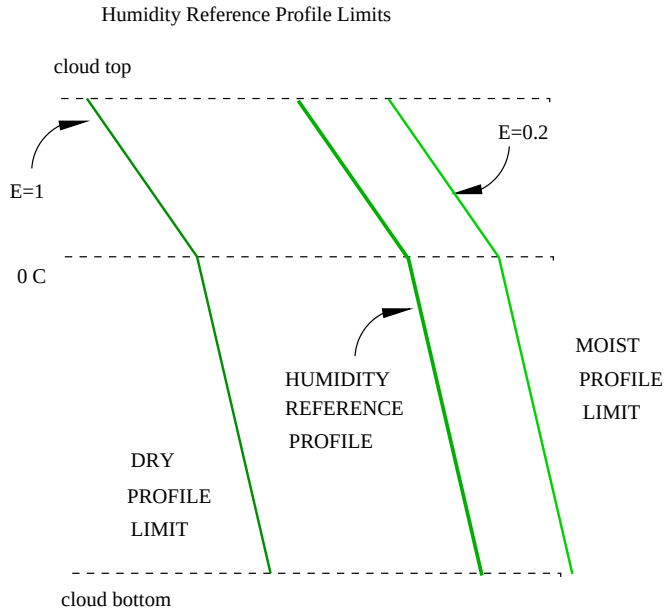

Fig. A1.6: Schematic presentation of the evolution of a humidity reference profile as *E* deceases during a convective episode.

From the empirical data and analysis of many forecasts Janjic suggested revision of the values for *dsps* , presented in the **Table A1.2**, for three characteristic levels with different values for the "*fast*" profiles and for the "*slow*" ones (0.6-.85 of the fast ones) and different over land and sea:

Char. cloud level	notation	Fast *dsp* for sea	Fast *dsp* for land
		mb's	mb's
Top	dsp_{top}	-18.75	-22.50
Freezing	$dsp_{freezing}$	-58.75	-70.50
Bottom	dsp_{bottom}	-38.75	-48.44

Table A1.2: The new values of *dsp* for the characteristic level suggested by Janjić-

Modified shallow convection

In comparison with the original BM scheme Janjić (1994) modified the shallow convection scheme as well. The first modification concerns the position of the cloud top for the model points where the swap was done. Now it is calculated from the humidity profile as the level with large vertical gradient. The same procedure was then extended to all shallow convection points to have the same treatment in all points. This was done in accordance with recommendation made by Betts. The largest modification concerns the construction of the humidity profiles. Instead of prescribing some fixed values for *dsp's*, the enforcement of the positive entropy change was built in the process of obtaining the humidity profile. The profile of the specific humidity is of the form

$$q_{ref}(p) = q_{ref,top} + c\left[Q(p) - Q(p_{top})\right]$$

After looking into several other possibilities $Q(p)$ was set to T_{ref}. It was also evident from data that total entropy change was small number which together with function $Q(p)$ enables us in determining the $q_{ref,top}$. If we calculate separately change of entropy from the temperature change and from the specific humidity change and assume that

$$\Delta S_q = -(1+\mu)\Delta S_T \quad , with \quad \mu = 0.05$$

we can get the reference profiles for the shallow convection. Still even with profiles obtained in this way there were occasions that rendered posterior corrections. For instance positive entropy change from the temperature, evolution of the temperature profile so that it becomes to close to the isothermal profile, negative gradients of the specific humidity, excessive instability of the virtual potential temperature (≤ .3 ° K, again Betts suggestion) and upper limit of 500 mb was set to the position of the cloud top.